Analysis of positron asymmetries using September data

R. Dollan, H. Kolanoski, T. Lohse, *HU Berlin*
K. Laihem, S. Riemann, A. Schälicke, *DESY, Zeuthen*

E-166 note, February 28, 2006

Abstract

In September 2005 the E166 experiment had the second period of data taking. Measurements of positron asymmetries have been performed at 5 different energies of the positrons. In addition one electron asymmetry has been determined, and the effect of operating the undulator with ferro-fluid has been investigated.

For the energy point with the highest statistics we find for the central crystal of the CsI calorimeter an asymmetry of $A_5 = (1.03 \pm 0.08)\%$, where the error includes systematic uncertainties. Extending the analysis to the complete CsI calorimeter, the result becomes $A_{all} = (0.91 \pm 0.07)\%$.

Contents

1 Introduction

In this note we derive asymmetries from signals measured with the central crystal of the Cs(I) calorimeter for the 7 different experimental settings of the E166 run in September 2005. This analysis represents a sequel of the E166 note in September [1]. Special emphasis is given to the correct determination of statistical and systematic errors. In total, data of more than 8 million beam pulses have been included in the analysis, corresponding to approximately 220 hours run time. For the setup with highest statistics we examine the impact of including all crystals of the calorimeter into the analysis.

First results have been presented at the E166 meeting in November 2005 [2–5], and showed good agreement. In December 2005, G. Alexander and E. Reinherz-Aronis published a note on an analysis of the data with an alternative approach [6].

The structure of the paper is the following. First, in Sec. 2 the general procedure is outlined. The subsequent sections concentrate on different aspects of the analysis. In Sec. 7, the systematic errors are discussed and quantified. Preliminary results are given in Sec. 8. At the end, in Sec. 9 we give an outlook how the analysis can be extended to the whole calorimeter, and summarize our findings in Sec. 10. An interested reader will find further details in the appendix.

2 General analysis procedure

In general the data have the following structure: For each spectrometer setting, a number of "*super-runs*" is taken. One *super-run* consists of cycles with usually 3000 beam pulses. In an automatic procedure the polarity of the analyzer magnet is flipped between each cycle. Half of the events in one cycle are "background" events, i.e. the undulator was off at these beam pulses. The other half are "signal" events, which means the undulator was on and all detectors recorded signal + background. The data have the structure with alternating "signal" and "background" events.

Our analysis follows a cycle-based approach. The procedure is the following:

- For this analysis we employ the central CsI crystal only, and use the so called "low sensitivity"(12bit)-data of "gain1". In the "high sensitivity" mode we discovered an overflow for a number of runs, therefore a part of the distribution of the energy deposition is cut off. Hence we do not use these data for the asymmetry determination.
- First the background conditions are determined to fix cut parameters. This ensures to select only events recorded under stable beam conditions.
- In a second step all events are normalized to the beam current. That means every event (background and signal) is divided by the readings of *tor6130*.
- Then, the subtraction of background from signal + background events is performed.
- The background subtracted signal is multiplied with the calibration constant corresponding to the CsI-crystal. For an analysis of the central crystal only, this step is optional.
- Asymmetries are determined on a cycle-to-cycle basis: a pair of adjacent cycles with opposite magnet polarity is selected and the asymmetry is calculated from the corresponding energy depositions.

- Finally, all the single asymmetries for one positron (electron) momentum are used to determine a global asymmetry for this momentum point.

In the following sections we discuss the details of this procedure.

3 Data selection

3.1 Selection of runs and cycles

The asymmetries are always derived from a pair of adjacent cycles with opposite magnet polarity in the way, that the mean energy deposition in the central CsI-Crystal of the "positive" cycle is subtracted from the mean energy deposition of the "negative" cycle. These cycle pairs are considered together in all steps of the analysis.

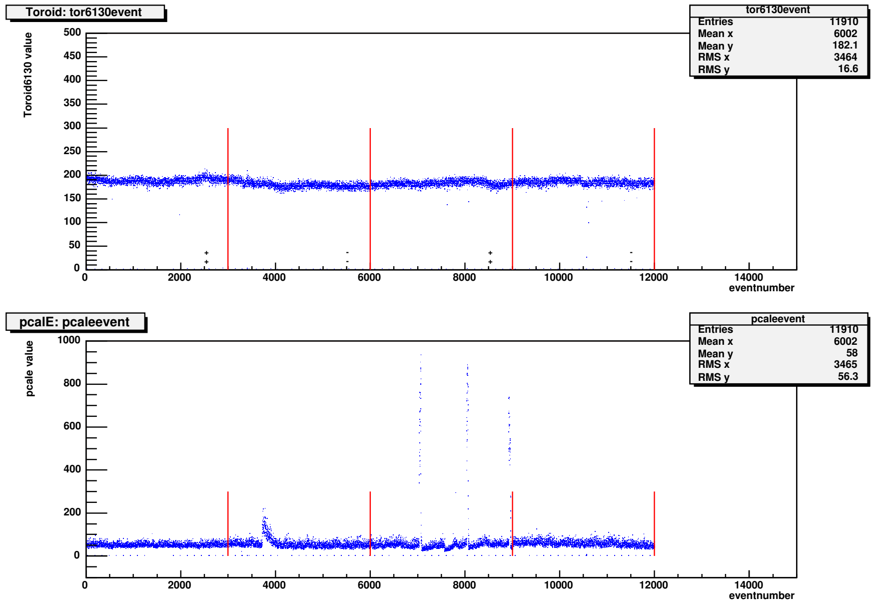

Figure 1: *The* tor6130*-signal vs. time (top) and the* pcalE*-signal vs. time (bottom). Example of run with four cycles (Run 2196)*

At first, the runs/cycles are selected depending on the experimental setup. We have five spectrometer/lens settings in the September data, among them are also the electron data and the data from the last period, where the undulator was filled with ferro-fluid. We believe, the latter data have to be analyzed separately. This results in the following data sets:

Spectrometer [A]	Lens [A]	mode
100	220	positrons
120	260	positrons
140	340	positrons
160	360	positrons
160	360	electrons
180	374	positrons
180	374	positrons - undulator filled with ferro-fluid

The lens-, spectrometer- and target settings are taken from the mcc-scp data in the raw files. Also the polarity of the analyzer magnets is taken from these data. The result is a database of runs/cycles with their respective settings (see also Elog entry Run/163 and Elog entry Run/164).

Note: For the spectrometer current 140A the data set can be divided in two running periods. For the analysis the second running period was chosen. We observed large background fluctuations in the first period. A complete list of the selected runs can be found in appendix A.

3.2 Determination of run conditions

For the quality check the two adjacent cycles to be considered for the asymmetry determination are treated as one. The readings of the *tor6130* of both cycles are filled into a single histogram. A similar histogram is created for the background monitor *pcalE*. A Gauss function is fitted to these distributions and its mean, width and RMS are derived (Figure 2 and Figure 3). The ratio $q = RMS/Mean$ of the distributions is a good quality criterion and can be used as a measure for the stability of the conditions (beam current and background) during the two cycles.

3.3 Applied cuts

The cut values are derived from the fit of the distribution of the *tor6130*- and the *pcalE*-readings (see section 3.2 above). The following cuts are applied:

Cut1: A general cut, that is applied always, is a cut on the beam current (*tor6130*): Only those events from both cycles are selected, that have a beam current value within a 3σ-range around the mean beam current of both cycles. This cut is used to select events that are recorded under stable beam current conditions (cf. Figure 2).

Cut2: An additional cut on the *pcalE* values selects a 1σ-range around the mean value of the combined *pcalE* distribution of both cycles. This cut selects events with the same or at least comparable background conditions (cf. Figure 3).

Cut	value	range
1	*tor6130*	(Mean $\pm$ 3σ)
2	*pcalE*	(Mean $\pm$ 1σ)

4 Normalization to toroid *tor6130*

In the beginning of the September run, a toroid scan was performed to determine an optimal current for the background conditions existing at that time. In these runs (run 1966-1970, and run 1975-1991) the current has been varied between $10 \cdot 10^9$ and $0.5 \cdot 10^9$ e^- per bunch, while other parameters like alignment of undulator and beam, energy set-point etc. have been kept the same.

The CsI signal of a single run (or cycle) with relative stable current does not show a correlation with the current. A possible dependence on the current is washed out by the large (uncorrelated) fluctuation of the background. If on the other hand the current changes during one run (cf. June run 1496) or between runs (see Figure 4), CsI-toroid correlation becomes visible.

This leads to three different analysis options:

a) normalize the CsI energy to the toroid value for each beam pulse,

b) normalize the mean CsI energy to the mean toroid value for each data cycle,

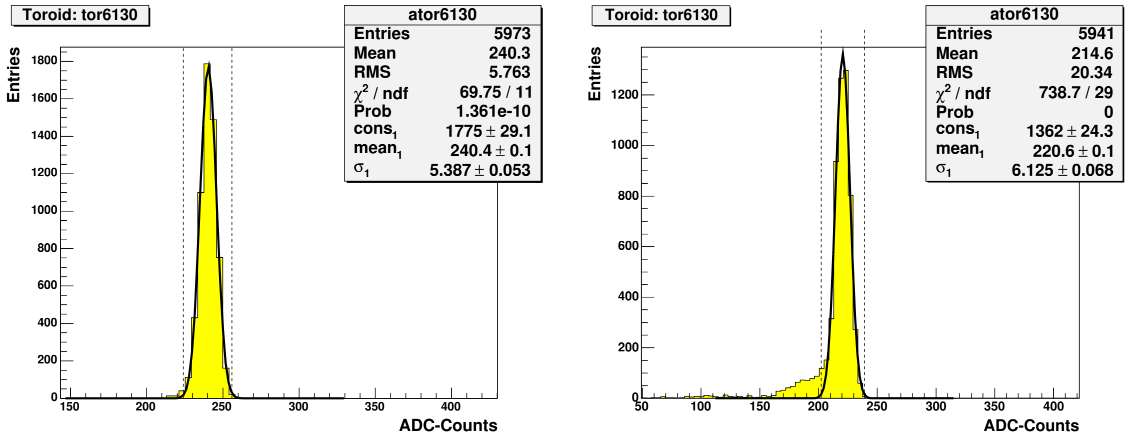

Figure 2: *The distribution in the* tor6130. *Two adjacent cycles (polarity minus and plus) are combined in the histograms. Left: run 2548 cycle 0 and cycle 1 - stable conditions. Right: run 2555 cycle 4 and cycle 5 - more unstable conditions. The vertical lines indicate the* $\pm 3\sigma$*-range used for the analysis.*

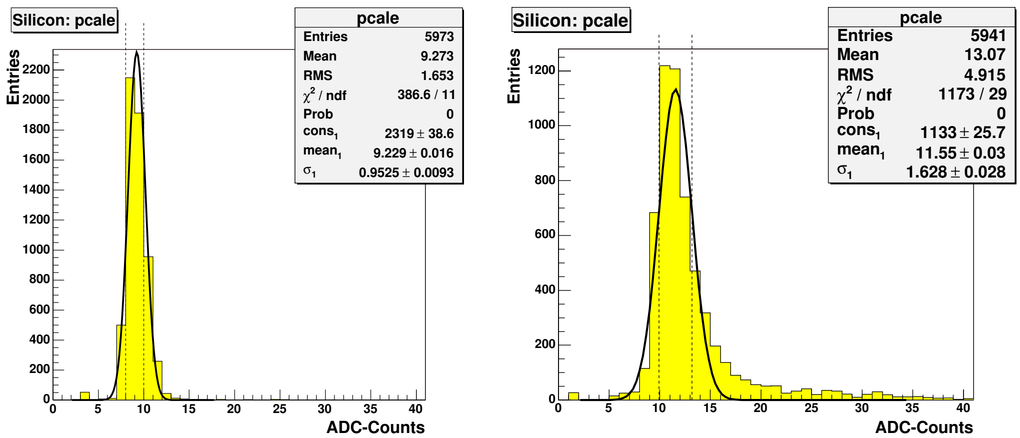

Figure 3: *The distribution in the* pcalE. *Two adjacent cycles (polarity minus and plus) are combined in the histograms. Left: run 2548 cycle 0 and cycle 1 - stable background conditions. Right: run 2555 cycle 4 and cycle 5 - more unstable background conditions. The vertical lines indicate the* $\pm 1\sigma$*-range used for the analysis.*

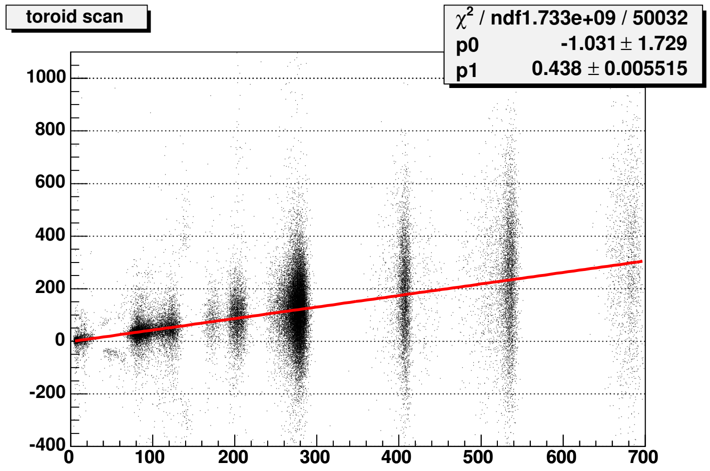

Figure 4: *The CsI signal vs. toroid values. Due to the background fluctuations the correlations between toroid values and CsI signals are normally washed out. They become visible in case of larger changes of the toroid current between runs or even during runs.*

c) do not normalize at all.

The resulting asymmetries, A, for a spectrometer current of 140 A (Method C introduced in [1], 3σ toroid cut, see section 3.3) are summarized in Table 1:

Table 1: *Asymmetries in percent measured in the central crystal using the 3 different analysis options explained above.*

	A [%]	ΔA [%]	χ^2/ndf
a	0.98804	0.05558	864/225
b	0.99798	0.05573	874/225
c	0.90771	0.05575	1288/225

With 3σ cuts on the toroid signal the toroid values within a cycle are very stable, and hence there is no significant difference in the pure statistical error for options a), b) and c). However, without toroid normalization, option c), the χ^2/ndf increases drastically and the calculated asymmetry is significantly lower than the values from methods a) and b). Taking into account that all methods use exactly the same data, this observation indicates a mismatch in the toroid current between *plus* and *minus* cycles.

Our conclusion is to apply option a), i.e. for each *signal* and *background* event, the CsI energy deposition is normalized to the corresponding toroid signal. Option b) can be assumed to yield similar results, while option c) should not be used or only if additional measures are taken like e.g. dividing up in periods of constant current.

5 Background subtraction and energy deposition in the crystal

In the following, "signal" means an "undulator-on-event", which is actually signal+background, and "background" means an "undulator-off-event", what is pure background. We are using different methods of the background subtraction as described in the following. All the events

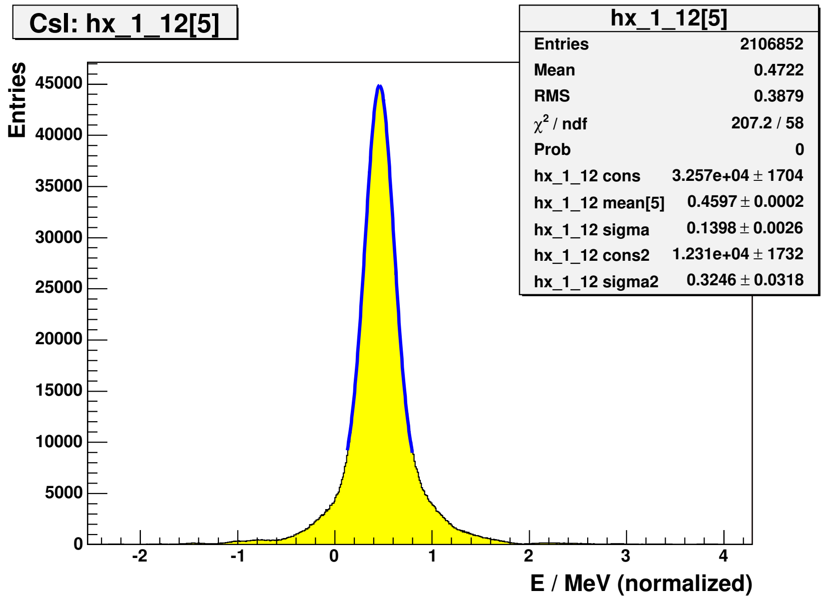

Figure 5: *The normalized energy deposition in the central CsI-crystal; Meth. D; "double Gaussian" fit with a fit range of* $\pm 2\sigma$.

are normalized to the beam current that means that every (signal- or background-) event is divided by the reading of *tor6130* for this event (cf. section 4).

5.1 Method "D"

Every background event of a cycle is subtracted from every signal event of a cycle and all the results are filled into one histogram.

$$< S - B >= \frac{1}{n_s n_b} \sum_{i=1}^{n_s} \sum_{j=1}^{n_b} (s_i - b_j) \tag{1}$$

A resulting distribution is shown in Figure 5. The mean is determined via a fit of the peak region (see also [1]).

5.2 Method "C1"

A signal has to be surrounded by two background events, one before and one after (after cuts). This assures, that the compared signal and background events are in the same time regime even after cuts. Each of these two background events is subtracted from the signal and the two results are filled into a histogram. In this way the background subtracted signal is less sensitive on any time dependence of the background and the pairing of signal and background events does not matter,

$$< S - B >= \frac{1}{2n_s} \sum_{i=1}^{n_s} (s_i - b_{i-1}) + (s_i - b_{i+1}) \ . \tag{2}$$

An example of the resulting distributions is shown in Figure 6.

5.3 Fit procedure

The sum of two Gauss functions ("double Gaussian") was chosen as fit function for the energy distribution. In an iterative procedure the start parameters and the fit range for the final fit are determined. From Figure 6it can be seen, that the "double Gaussian" describes the obtained distribution much better than a "single Gaussian".

The energy depositions $E^{\pm}$ are the peak positions of the final fit. The errors are calculated from the width (full width at half maximum) of the fit function and the number of events contributing to the fit are :

$$\Delta E^{\pm} = \frac{\sigma_E}{\sqrt{2}} \cdot \sqrt{\frac{1}{n_s} + \frac{1}{n_b}} \,, \quad \text{with} \quad \sigma_E = \frac{FWHM}{2.35} \,, \tag{3}$$

where n_s and n_b denotes the number of signal- and background events in the fit region, and σ_E is used as the width equivalent for the "double Gaussian".

6 Asymmetry calculation

The asymmetries A_i are calculated from the mean energy deposition in the CsI-Calorimeter. E_i^- and E_i^+ are the mean energy depositions in the central crystal for the cycle with "negative" and "positive" magnet polarity, respectively. The asymmetry for each cycle pair is then

$$A_i = \frac{E_i^- - E_i^+}{E_i^- + E_i^+} \,, \tag{4}$$

with the error

$$\Delta A_i = \frac{2}{\left(E_i^- + E_i^+\right)^2} \cdot \sqrt{\left(E_i^+ \, \Delta E_i^-\right)^2 + \left(E_i^- \, \Delta E_i^+\right)^2} \,, \tag{5}$$

where the errors ΔE_i^- and ΔE_i^+ are determined as described in section 5.3.

The value for the asymmetry A for the respective energy point is determined by a linear fit to all single asymmetries A_i taking the errors into account. This method is equivalent to calculating a weighted mean,

$$\langle A \rangle = \frac{\sum_{i=1}^{N} \frac{1}{\Delta A_i{}^2} A_i}{\sum_{i=1}^{N} \frac{1}{\Delta A_i{}^2}} \,, \tag{6}$$

and its error

$$\Delta \langle A \rangle = \left(\sum_{i=1}^{N} \frac{1}{\Delta A_i{}^2} \right)^{-\frac{1}{2}} \,. \tag{7}$$

The χ^2/ndf can be used as a quality measure of the result. An example fit is shown in Figure 7. Examples for all methods can be found in appendix B.

The asymmetry values are calculated using method "C1" and "D" and with different combinations of cuts. The impact of Cut2 can be seen in Figure 7 and Figure 8 as well as in Table 2.

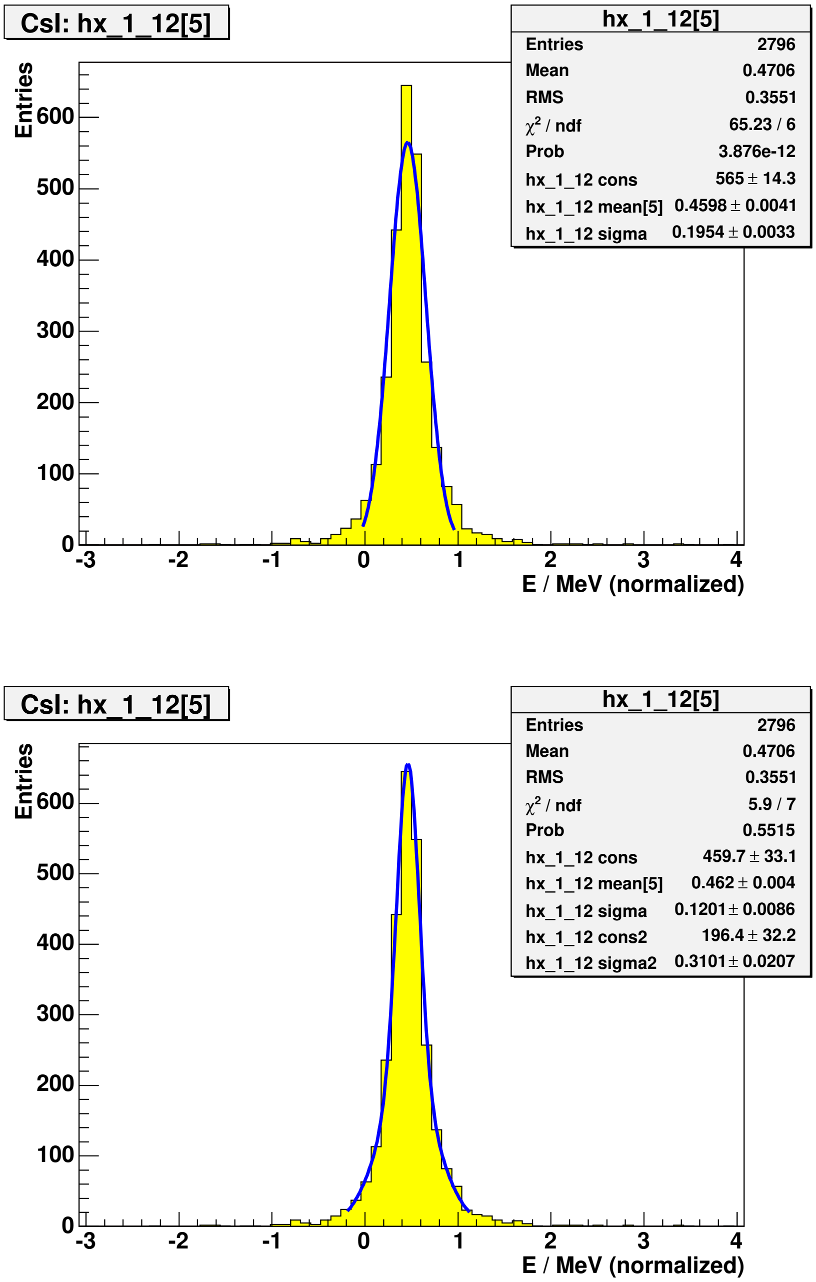

Figure 6: *The normalized energy deposition in the central CsI-crystal. Meth. C1; Top: a single Gaussian with a range of $\pm 1.5\sigma$ is used as fit function. Bottom: a "double Gaussian" fit with a fit range of $\pm 2\sigma$ is applied to the same distribution.*

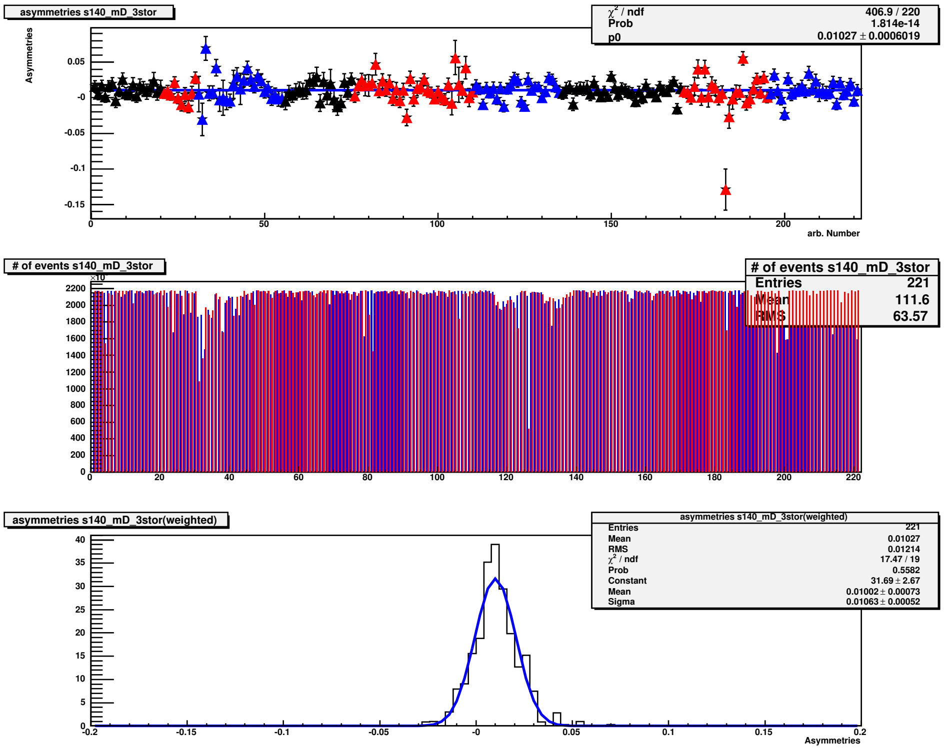

Figure 7: *The single asymmetries A_i for the Spec:140 setting - background subtraction method D + Cut1. Top: The single asymmetries with their errors. Middle: The number of "survived" events contributing to the asymmetry determination. Bottom: Histogram of the single asymmetries weighted according to Eq.* (11)*.*

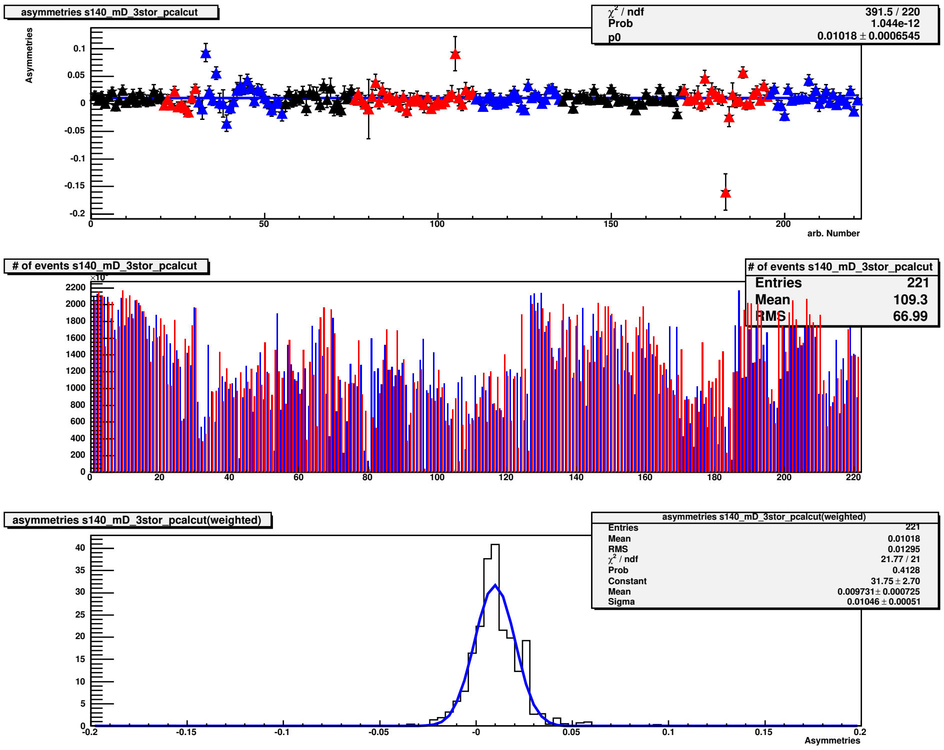

Figure 8: *Same plots as in Figure 7, but after additional application of Cut2.*

Table 2: *Asymmetries A for the Spectrometer 140A setting depending on the background subtraction method and the applied cuts. The figure of merit in the last column should be minimal.*

	A [%]	ΔA [%]	χ^2/ndf	$\sqrt{\chi^2/ndf} \cdot \Delta\mathrm{A}$
meth. C1	1.07	0.05	765.4 / 220	0.093
meth. C1 + Cut2	1.09	0.07	598.3 / 220	0.120
meth. D	1.03	0.06	406.9 / 220	0.082
meth. D + Cut2	1.02	0.07	391.5 / 220	0.093

7 Quantification of systematic uncertainties

7.1 χ^2 analysis

In general, the calculation of the asymmetries requires that the *plus* and *minus* measurements are performed under equivalent conditions. Variations that connot be compensated will unavoidably lead to systematic errors. This section is devoted to a detailed analysis of systematic uncertainties.

In our analysis we follow a cycle-based approach. This means that each cycle pair provides an independent asymmetry measurement. The statistical error of an individual asymmetry is derived from properties of the energy distribution (width, number of signal events). The total asymmetry and its statistical uncertainty is then given by the weighted mean formulae Eqs. (6) and (7).

On the other hand, a good measure for the total uncertainty is given by the variance of all individual asymmetries A_i. This fact offers the possibility to separate systematic and statistical uncertainties. The relevant measure is χ^2/ndf. In general, $\chi^2/ndf < 1$ indicates that the individual errors are maybe overestimated, and for $\chi^2/ndf > 1$ the errors are possibly too small[1].

7.2 Figure of merit

We define a *figure of merit* to be the total uncertainty including the systematical error:

$$\Delta A_\chi = \sqrt{\frac{\chi^2}{ndf}} \Delta A \,. \tag{9}$$

This is, of course, only an approximation to the total uncertainty, but it already helps to determine the appropriate analysis method.

In addition to the statistical error, the systematical uncertainties have to be quantified too. Therefore we perform three basic tests:

- check the stability of the asymmetries with respect to cuts, and analysis methods,

[1]In fact, χ^2 follows a distribution $P(\chi^2; n)$. With n is the number of degrees of freedom, and $\Gamma(x)$ the standard gamma function, it can be written as

$$P(\chi^2; n) = \frac{2^{-n/2}}{\Gamma(n/2)} \chi^{n-2} e^{-\chi^2/2}. \tag{8}$$

To make a judgement about a given χ^2 the relevant quantity is the integral of $P(\chi^2; n)$, the so-called χ^2 *probability*.
For practical purpose it is more convenient to use $\sqrt{2\chi^2}$, which offers a reasonable approximation to a Gauss function with a mean of $\sqrt{2n-1}$ and a width equal to one (for $n > 30$). For a more rigorous discussion of the properties of $P(\chi^2; n)$ we refer to standard textbooks on statistics, e.g. [7].

- check the effect of rejecting obvious outliers,
- look into other crystals.

7.3 Quality criterion

In the following, the impact of the quality criterion q on the asymmetries A is studied (compare section 3.2). Pairs of cycles with a q larger than a certain value were rejected. Table 3 shows the resulting asymmetry depending on a cut on q. The fit to the asymmetries A_i of the cycle pairs that "survived" the cut on q is shown in Figures 24 to 26.

Table 3: *The impact of the quality criterion $RMS/Mean$ of the* pcalE *distribution. q=max means, no cycle pairs were rejected, q<2,1,0.8 means cycle pairs with q large than 2,1,0.8 were rejected.*

	$RMS/Mean$	A [%]	ΔA [%]	χ^2/ndf	ΔA_χ [%]
Meth. D	q=max	1.03	0.06	406.9 / 220	0.08
Meth. D	q<2	1.02	0.06	398.7 / 213	0.08
Meth. D	q<1	1.04	0.07	294.2 / 161	0.10
Meth. D	q<0.8	1.11	0.08	233.3 / 135	0.10

7.4 Rejection of outliers

In order to investigate the stability of the results we define a *"outlier rejection"* stategy. The procedure consists of the following steps:

a) First determine all individual contributions χ_i^2 to the total χ^2, with

$$\chi_i = \frac{A_i - \langle A \rangle}{\Delta A_i^2} \; . \tag{10}$$

b) Select the cycle with the largest χ_i^2 and reject the complete *super-run*, i.e. use χ_i^2 as indicator for "bad" runs.

c) Evaluate the figure of merit ΔA_χ according to Eq. (9).

d) Continue with step a) to c) until ΔA_χ is a minimal.

The effect of this approach on mean and error of the asymmetry is summarized in table 4.

An alternative approach to the *"outlier rejection"* is given by filling all single asymmetries A_i in a histogram with a weight

$$w_i = \frac{1}{\Delta {A_i}^2} \Big(\sum_{i=1}^{N} \frac{1}{\Delta {A_i}^2} \Big)^{-1} \; . \tag{11}$$

By construction the mean of this histogram is equivalent to the weighted mean $\langle A \rangle$, cf. (6). This distribution can now be fitted with a Gauss function, and is used to derive an asymmetry $A_{\bar{\chi}}$ and its error $\Delta A_{\bar{\chi}}$.

Table 4: *The rejection of outliers. The runs in the second column are rejected in addition to the line above.*

	+ rej. runs	A [%]	ΔA [%]	χ^2/ndf	ΔA_χ [%]	$A_{\bar{\chi}}$ [%]	$\Delta A_{\bar{\chi}}$ [%]
Meth. D	(no rejection)	1.027	0.060	406.9 / 220	0.082	1.002	0.073
Meth. D	2609	1.021	0.061	378.3 / 215	0.081	1.019	0.074
Meth. D	+ 2607	1.040	0.061	347.7 / 210	0.079	1.046	0.073
Meth. D	+ 2625	1.049	0.062	322.1 / 201	0.079	1.041	0.074
Meth. D	+ 2553	1.047	0.063	306.1 / 196	0.079	1.053	0.076
Meth. D	+ 2600	1.052	0.064	289.8 / 191	0.079	1.042	0.076
Meth. D	+ 2558	1.023	0.065	273.6 / 186	0.078	1.011	0.075
Meth. D	+ 2573	1.030	0.065	258.7 / 181	0.078	1.014	0.076
Meth. D	+ 2586	1.038	0.066	237.2 / 176	0.077	1.000	0.075
Meth. D	+ 2582	1.051	0.068	227.3 / 171	0.078	1.027	0.076
Meth. D	+ 2585	1.072	0.069	216.5 / 166	0.079	1.041	0.077

8 Preliminary Results

In the following the results for the different experimental setups are listed. To compare the results of the different methods and cuts also the $\Delta A_\chi = \sqrt{\chi^2/ndf} \cdot \Delta \mathrm{A}$ as a figure of merit is given.

Table 5: *Asymmetries A for the Spectrometer 100A setting depending on the background subtraction method and the applied cuts. In addition the $A_{\bar{\chi}}$ and the $\Delta A_{\bar{\chi}}$ are shown.*

	A [%]	ΔA [%]	χ^2/ndf	ΔA_χ [%]	$\mathrm{A}_{\bar{\chi}}$ [%]	$\Delta \mathrm{A}_{\bar{\chi}}$ [%]
Meth. C1	0.62	0.14	331.4 / 203	0.17	0.61	0.16
Meth. C1 + Cut2	0.41	0.20	374.1 / 203	0.27	0.55	0.23
Meth. D	0.57	0.17	180.2 / 203	0.16	0.58	0.14
Meth. D + Cut2	0.54	0.18	251.5 / 203	0.20	0.42	0.17

Table 6: *Asymmetries A for the Spectrometer 120A setting depending on the background subtraction method and the applied cuts. In addition the $A_{\bar{\chi}}$ and the $\Delta A_{\bar{\chi}}$ are shown.*

	A [%]	ΔA [%]	χ^2/ndf	ΔA_χ [%]	$\mathrm{A}_{\bar{\chi}}$ [%]	$\Delta \mathrm{A}_{\bar{\chi}}$ [%]
Meth. C1	0.88	0.07	498.0 / 185	0.11	0.89	0.10
Meth. C1 + Cut2	0.89	0.09	426.5 / 185	0.14	0.86	0.12
Meth. D	0.88	0.08	268.5 / 185	0.10	0.91	0.09
Meth. D + Cut2	0.96	0.09	284.3 / 185	0.11	0.95	0.10

Table 7: *Asymmetries A for the Spectrometer 140A setting depending on the background subtraction method and the applied cuts. In addition the $A_{\bar{\chi}}$ and the $\Delta A_{\bar{\chi}}$ are shown.*

	A [%]	ΔA [%]	χ^2/ndf	ΔA_χ [%]	$A_{\bar{\chi}}$ [%]	$\Delta A_{\bar{\chi}}$ [%]
Meth. C1	1.07	0.05	765.4 / 220	0.10	1.07	0.08
Meth. C1 + Cut2	1.09	0.07	598.3 / 220	0.11	1.11	0.09
Meth. D	1.03	0.06	406.9 / 220	0.08	1.00	0.07
Meth. D + Cut2	1.02	0.07	391.5 / 220	0.09	0.97	0.07

Table 8: *Asymmetries A for the Spectrometer 160A (positrons) setting depending on the background subtraction method and the applied cuts. In addition the $A_{\bar{\chi}}$ and the $\Delta A_{\bar{\chi}}$ are shown.*

	A [%]	ΔA [%]	χ^2/ndf	ΔA_χ [%]	$A_{\bar{\chi}}$ [%]	$\Delta A_{\bar{\chi}}$ [%]
Meth. C1	0.84	0.09	575.5 / 165	0.16	0.81	0.12
Meth. C1 + Cut2	0.83	0.07	644.5 / 165	0.13	0.82	0.09
Meth. D	0.83	0.08	417.1 / 165	0.12	0.85	0.09
Meth. D + Cut2	0.88	0.08	472.7 / 165	0.14	0.80	0.10

Table 9: *Asymmetries A for the Spectrometer 160A (electrons) setting depending on the background subtraction method and the applied cuts. In addition the $A_{\bar{\chi}}$ and the $\Delta A_{\bar{\chi}}$ are shown.*

	A [%]	ΔA [%]	χ^2/ndf	ΔA_χ [%]	$A_{\bar{\chi}}$ [%]	$\Delta A_{\bar{\chi}}$ [%]
Meth. C1	1.35	0.04	399.6 / 141	0.07	1.31	0.07
Meth. C1 + Cut2	1.31	0.05	426.9 / 141	0.09	1.26	0.08
Meth. D	1.31	0.05	251.4 / 141	0.06	1.30	0.10
Meth. D + Cut2	1.32	0.05	388.8 / 141	0.08	1.28	0.08

Table 10: *Asymmetries A for the Spectrometer 180A setting depending on the background subtraction method and the applied cuts. In addition the $A_{\bar{\chi}}$ and the $\Delta A_{\bar{\chi}}$ are shown.*

	A [%]	ΔA [%]	χ^2/ndf	ΔA_χ [%]	$A_{\bar{\chi}}$ [%]	$\Delta A_{\bar{\chi}}$ [%]
Meth. C1	0.96	0.16	142.5 / 63	0.24	1.06	0.17
Meth. C1 + Cut2	1.06	0.20	125.7 / 63	0.28	0.99	0.24
Meth. D	0.89	0.18	81.3 / 63	0.21	0.96	0.18
Meth. D + Cut2	0.86	0.20	96.8 / 63	0.25	0.76	0.20

Table 11: *Asymmetries A for the Spectrometer 180A (Ferro-fluid) setting depending on the background subtraction method and the applied cuts. In addition the $A_{\bar{\chi}}$ and the $\Delta A_{\bar{\chi}}$ are shown.*

	A [%]	ΔA [%]	χ^2/ndf	ΔA_χ [%]	$A_{\bar{\chi}}$ [%]	$\Delta A_{\bar{\chi}}$ [%]
Meth. C1	0.93	0.11	462.9 / 103	0.23	1.06	0.19
Meth. C1 + Cut2	0.64	0.15	371.5 / 103	0.28	0.72	0.24
Meth. D	0.98	0.13	271.7 / 103	0.21	0.99	0.20
Meth. D + Cut2	0.84	0.14	328.2 / 103	0.26	0.92	0.25

9 Whole calorimeter asymmetry

9.1 Check for systematic energy shifts in the calorimeter

To assure that the observed asymmetry in the central crystal has its origin not in a shift of the beem but in polarization, we have analysed asymmetries of adjacent crystals.

The table 12 gives an example for spectrometer current 140 A. For negative/positive analyzer polarity the energy depositions (normalized to toroid) in MeV/ADC are listed for all 9 crystals. The error estimate is pure statistical, and ignores the uncertainty of the calibration.

Table 12: *Energy deposition in the nine crystals normalized to toroid values for negative and positive analyzer polarity.*

E^- [MeV/ADC]

0.05035(53)	0.1559(13)	0.0904(8)
0.2004(25)	0.4729(33)	0.1731(14)
.07907(72)	0.1943(17)	0.0863(11)

E^+ [MeV/ADC]

0.04926(52)	0.1528(12)	0.08947(87)
0.1955(24)	0.463(3)	0.1685(12)
0.07899(72)	0.1916(17)	0.0856(11)

Table 13: *Asymmetries, A_i, in percent measured in each of the nine CsI crystals.*

A_i in [%]

0.47(37)	1.04(20)	−0.04(40)
1.24(27)	1.03(8)	1.34(17)
0.08(34)	0.71(16)	0.79(36)

There is no indication of a shift in the calorimeter signals. The corresponding asymmetries, A_i, for each crystal are summarized in Table 13. The asymmetries measured in the outermost crystals are significantly below that in the central crystal. This is not surprising: Due to the geometry of the analyzer magnet with the ferromagnet and the following calorimeter the transmitting photons created in the reconversion target hit mainly the central crystal (see also next section).

9.2 Different approaches to look for a "whole calorimeter" asymmetry

First a **warning**:

- The analyzing power depends on the position of the crystals used in the analysis. For instance, due to geometry the four *"corner crystals"* (1,3,7,9) see only secondary radiation created in the iron of the analyzer magnet, in the lead shield of the magnet or in the magnet housing, and they do not detect primary radiation created in the reconversion target and transmitted through the magnetized iron. The analyzing power is only accessible through simulations. Thus, a determination of asymmetries in different crystals is a valuable check of the experimental setup as well as the reliability of the simulation.

In the following two different approaches to determine a "whole calorimeter" asymmetry are discussed.

a) *Sum approach*
The energy distributions of all crystals are summed for *signal* and for *background* events to calculate an overall asymmetry.

b) *Individual approach*
The individual asymmetries are determined for each crystal and combined regarding a correct weighting.

Sum approach

The total asymmetry is defined as

$$A = \frac{\sum L_i - \sum R_i}{\sum L_i + \sum R_i} \tag{12}$$

with $L_i = c_i * X_i^-$ and $R_i = c_i * X_i^+$ being the energy deposition in the individual crystals for negative and positive currents in the analyzer magnets. The calibration constants c_i relate the raw ADC counts to energy.

This approach has the problem, that each crystal is weighted equally, and the total error is dominated by the bad signal to background separation in the outer crystals, even though their impact on the total asymmetry should be smallest.

Individual approach

The basic idea of the *individual approach* is to calculate the asymmetries A_i for each crystal independently. Then the individual asymmetries are combined taking the signal level into account,

$$A = \frac{\sum_i L_i - \sum_i R_i}{\sum_i L_i + \sum_i R_i} = \frac{\sum_i (L_i - R_i)}{\sum_i (L_i + R_i)} \tag{13}$$

$$= \sum_i \frac{(L_i - R_i)}{\sum_j (L_j + R_j)} \tag{14}$$

$$= \sum_i \frac{(L_i + R_i)}{\sum_j (L_j + R_j)} \cdot \frac{(L_i - R_i)}{(L_i + R_i)} \tag{15}$$

$$= \sum_i d_i \cdot A_i \tag{16}$$

with

$$A_i = \frac{L_i - R_i}{L_i + R_i} = \frac{X_i^- - X_i^+}{X_i^- + X_i^+} \tag{17}$$

and

$$d_i = \frac{(L_i + R_i)}{\sum_j (L_j + R_j)} = \frac{E_i}{\sum_j (E_j)} \ . \tag{18}$$

Consequently an error in the outermost crystal will enter only with a weight corresponding to the relative energy deposition. The individual asymmetries A_i do not depend on the calibration constants. So it can be assumed that this approach gives more reliable results.

9.3 Combine asymmetries of all crystals

In section 9.1 it was shown that the energy deposition in the CsI calorimeter is symmetric within the current experimental uncertainties. Consequently it is possible to combine results from equivalent crystals. For this purpose we define three regions

- central $\equiv$ crystal 5,
- near $\equiv$ crystals 2, 4, 6 and 8,
- remote $\equiv$ crystals 1, 3, 7 and 9.

Following Eq. (16) the asymmetry can be written as

$$A = d_{\text{central}} \cdot A_{\text{central}} + d_{\text{near}} \cdot A_{\text{near}} + d_{\text{remote}} \cdot A_{\text{remote}} \tag{19}$$

with

$$d_{\text{central}} = d_5 \qquad A_{\text{central}} = A_5 \tag{20}$$

$$d_{\text{near}} = (d_2 + d_4 + d_6 + d_8) \qquad A_{\text{near}} = \frac{1}{4}(A_2 + A_4 + A_6 + A_8) \tag{21}$$

$$d_{\text{remote}} = (d_1 + d_3 + d_7 + d_9) \qquad A_{\text{remote}} = \frac{1}{4}(A_1 + A_3 + A_4 + A_9) \tag{22}$$

Replacing the coefficients d_i by the energy depositions E_i leads to the following expression

$$A = \frac{E_{\text{central}}}{E_{\text{sum}}} \cdot A_{\text{central}} + \frac{E_{\text{near}}}{E_{\text{sum}}} \cdot A_{\text{near}} + \frac{E_{\text{remote}}}{E_{\text{sum}}} \cdot A_{\text{remote}} \ . \tag{23}$$

Now the asymmetries can be determined by the procedure described in the main part of this note. The values for the energy depositions are given in sec. 9.1. In order to estimate the uncertainty of the calibration we use the fluctuation between 4 equivalent crystals to estimate the error on the energy deposition[2] and arrive at

$$E_{\text{central}} = 0.468 \pm 0.020 \ , \qquad A_{\text{central}} = 1.03 \pm 0.08 \ , \tag{24}$$

$$E_{\text{near}} = 0.716 \pm 0.040 \ , \qquad A_{\text{near}} = 1.08 \pm 0.10 \ , \tag{25}$$

$$E_{\text{remote}} = 0.305 \pm 0.036 \ , \qquad A_{\text{remote}} = 0.33 \pm 0.19 \ . \tag{26}$$

The total error is a combination of all single contributions.

$$\Delta A = |\partial_{E_c} A| \Delta E_{\text{central}} \oplus |\partial_{E_n} A| \Delta E_{\text{near}} \oplus |\partial_{E_r} A| \Delta E_{\text{remote}} \oplus |\partial_{A_c} A| \Delta A_{\text{central}} \oplus |\partial_{A_n} A| \Delta A_{\text{near}} \oplus |\partial_{A_r} A| \Delta A_{\text{remote}} \tag{27}$$

[2] The uncertainty of the calibration constant in the central crystal is assumed to coincide with the uncertainty of the calibration constant in the near region, i.e. $\Delta E_{\text{central}} = \Delta E_{\text{near}}/\sqrt{4}$

with

$$\partial_{E_c} A = (A_c - A_n)\frac{E_{\text{near}}}{E_{\text{sum}}^2} + (A_c - A_r)\frac{E_{\text{remote}}}{E_{\text{sum}}^2} = 0.080 \qquad \partial_{A_c} A = \frac{E_{\text{central}}}{E_{\text{sum}}} = 0.314 \tag{28}$$

$$\partial_{E_n} A = (A_n - A_c)\frac{E_{\text{central}}}{E_{\text{sum}}^2} + (A_n - A_r)\frac{E_{\text{remote}}}{E_{\text{sum}}^2} = 0.114 \qquad \partial_{A_n} A = \frac{E_{\text{near}}}{E_{\text{sum}}} = 0.481 \tag{29}$$

$$\partial_{E_r} A = (A_r - A_c)\frac{E_{\text{central}}}{E_{\text{sum}}^2} + (A_r - A_n)\frac{E_{\text{near}}}{E_{\text{sum}}^2} = -0.390 \qquad \partial_{A_r} A = \frac{E_{\text{remote}}}{E_{\text{sum}}} = 0.205 \tag{30}$$

Inserting these numbers in Eqs. (23) and (27) we obtain the combined asymmetry of all crystals and its uncertainty

$$A = 0.910 \tag{31}$$

$$\Delta A = 0.0016 \oplus 0.0045 \oplus 0.014 \oplus 0.025 \oplus 0.048 \oplus 0.039 \tag{32}$$

$$\Delta A^{\text{max}} = 0.132 \tag{33}$$

$$\Delta A^{\text{sqr}} = 0.068 \tag{34}$$

Here, ΔA^{max} denotes the maximum uncertainty from adding all contributions in ΔA, and ΔA^{sqr} is obtained by summing in quadrature. The total uncertainty is dominated by the errors on the individual asymmetries; the uncertainty of the energy depositions in the regions is less important.

A simple exercise can be performed by concentrating on the *central* and *near* region only. Then the result of such combined asymmetry has a slightly smaller uncertainty than that of the complete calorimeter

$$A^{\text{cn}} = 1.060\ , \qquad A^{\text{cn,max}} = 0.093 \qquad A^{\text{cn,sqr}} = 0.068\ . \tag{35}$$

With respect to the central crystal only, the uncertainty is improved by approximately a factor $1/\sqrt{2}$.

To conclude, all CsI crystals can be included in an asymmetry determination without loss of significance. However, this has to be combined with a determination of the *analyzing power* for the extended detector region. The presented calculation of the total asymmetry is meant to illustrate the statistical relevance of such an analysis. Final numbers may change slightly, if the individual asymmetries are reevaluated, or new calibration constants are available.

10 Summary and outlook

We presented an analysis of the E166 data measured in September 2005.

Several selection criteria and cuts have been checked in connection with two procedures to extract the final asymmetry measured in the central crystal. The asymmetry should not depend on the approach and should be optimized to reach both a low statistical and systematic error. Method D meets these requirements if the final positron asymmetry is taken as weighted mean of the individual asymmetries. A figure of merit is defined to assure a realistic evaluation of the uncertainty. Unknown contributions to the systematic error are considered by weighting the variance of the asymmetry with χ^2/ndf.

Another criterion for systematic effects and the reliability of our analysis is the symmetry of the measurements within the whole CsI calorimeter.

It is found for the spectrometer set point *spect:140* that the asymmetries form a symmetric pattern concerning the crystal position. Due to the geometry the outermost crystals are nearly insensitive to the reconverterted photons and the asymmetries are expected to be very small. Combining the asymmetries measured only in the four neighbours of the central crystals, we find an asymmetry of the same size and uncertainty as in the central crystal. The combination of the asymmetry measurements in the central crystal and its direct neighbours could improve the accuracy and will be done for the final analysis for all positron energies.

Potential improvements of our method concern the handling of uncertainties: Here, we considered all uncertainties as symmetric errors. This approximation should be checked to avoid overestimations of the negative error to the asymmetry. In particular, this is important for individual asymmetries with large errors.

The results of our analysis are summarized in Table 14 and shown for the central crystal in Figure 9.

Table 14: *Asymmetries measured at different spectrometer settings. The numbers of the CsI crystals used for the analysis are given in the last row.*

Spectrometer [A]	A [%]	ΔA [%]	# of CsI crystals
100	0.57	0.17	5
120	0.88	0.10	5
140	1.03	0.08	5
160	0.83	0.12	5
180	0.89	0.21	5
180, ferrofl.	0.98	0.21	5
140	1.08	0.10	2,4,6,8
140	1.06	0.07	2,4,5,6,8
140	0.91	0.07	$1-9$
160, e^-	1.31	0.06	5

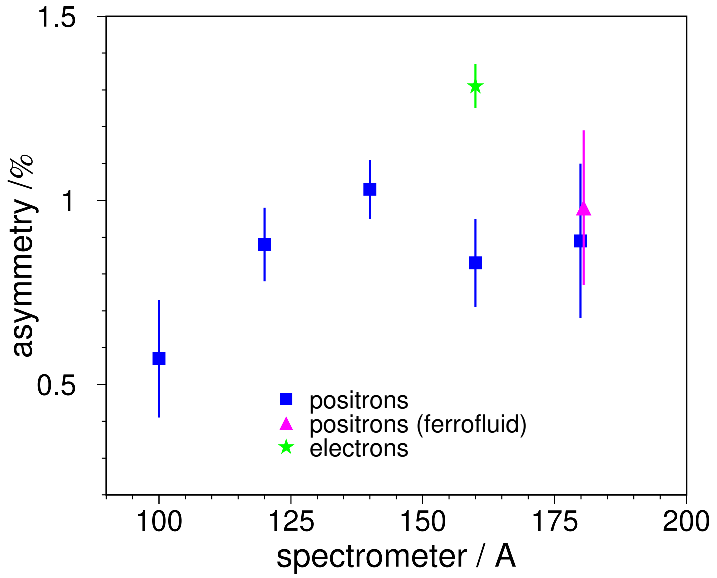

Figure 9: *Asymmetries measured at different spectrometer settings with the central crystal of the CsI calorimeter. The electron asymmetry is also shown.*

A Lists of runs/cycles

```
Spec:100 - runs:
2330 2332 2334 2335 2338 2340 2342 2344 2346 2347
2349 2350 2352 2354 2355 2357 2359 2366 2369 2371
2373 2375 2377 2380 2383 2386 2388 2390 2394 2395
2397 2404 2405 2408 2411 2413 2415 2416 2418 2419
2420 2422 2423 2425 2426 2428 2477

Spec:120 - runs:
2430 2440 2443 2444 2447 2449 2451 2453 2455 2457
2468 2469 2471 2473 2474 2478 2479 2481 2486 2497
2499 2501 2503 2506 2507 2509 2511 2516 2517 2518
2519 2521 2522 2524 2525 2527 2528 2530 2531

Spec:140second - runs:
2542 2545 2547 2548 2551 2553 2555 2558 2560 2562
2564 2565 2567 2570 2571 2573 2575 2577 2580 2582
2585 2586 2588 2589 2591 2592 2594 2595 2596 2599
2600 2602 2605 2607 2609 2612 2625 2627 2629 2630
2631

Spec:160positrons - runs:
2636 2637 2638 2640 2641 2642 2748 2749 2751 2753 2755
2757 2758 2760 2761 2763 2764 2766 2767 2770 2771 2773
2774 2776 2778 2780 2781 2783 2784 2786 2788 2790 2792
2794 2796

Spec:160electrons - runs:
2676 2678 2680 2681 2683 2685 2686 2689 2690 2692 2693
2695 2696 2697 2698 2700 2701 2703 2705 2707 2709 2711
2713 2737 2739 2741 2742 2744 2745

Spec:180 - runs:
2803 2805 2809 2812 2814 2816 2818 2819 2822 2823 2825
2826 2827

Spec:180Ferrofluid - runs:
2854 2856 2859 2862 2865 2867 2868 2870 2871 2873 2874
2876 2877 2878 2880 2881 2883 2884 2888 2889 2894
```

B Graphs and figures

B.1 Method C1/D + Cut1 with and without Cut2

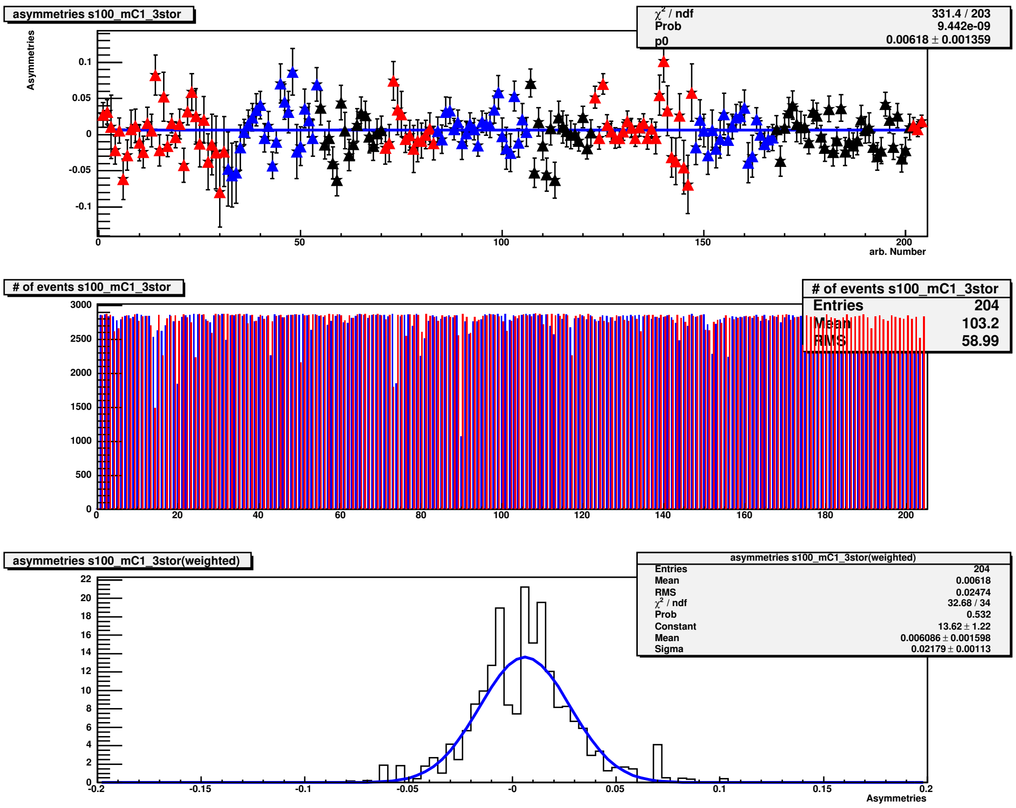

Figure 10: *The single asymmetries for the Spec:100 setting - background subtraction method C1 + Cut1. Top: The single asymmetries with their errors. Middle: The number of "survived" events contributing to the asymmetry determination. Bottom: Histogram of the single asymmtries weighted according to Eq.* (11)*.*
Color index: Top: black = owl shift, red = day shift, blue = swing shift. Middle: blue = "negative" cycle, red = "positive" cycle.

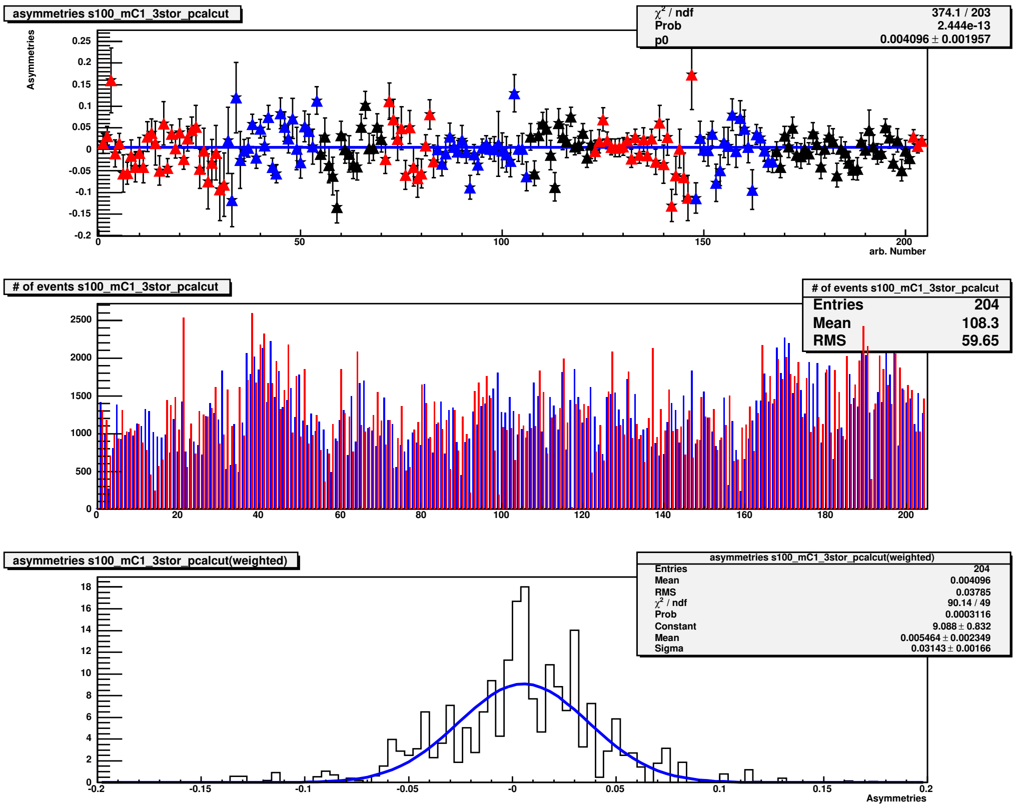

Figure 11: *Same plots as in Figure 10, but after additional application of Cut2.*

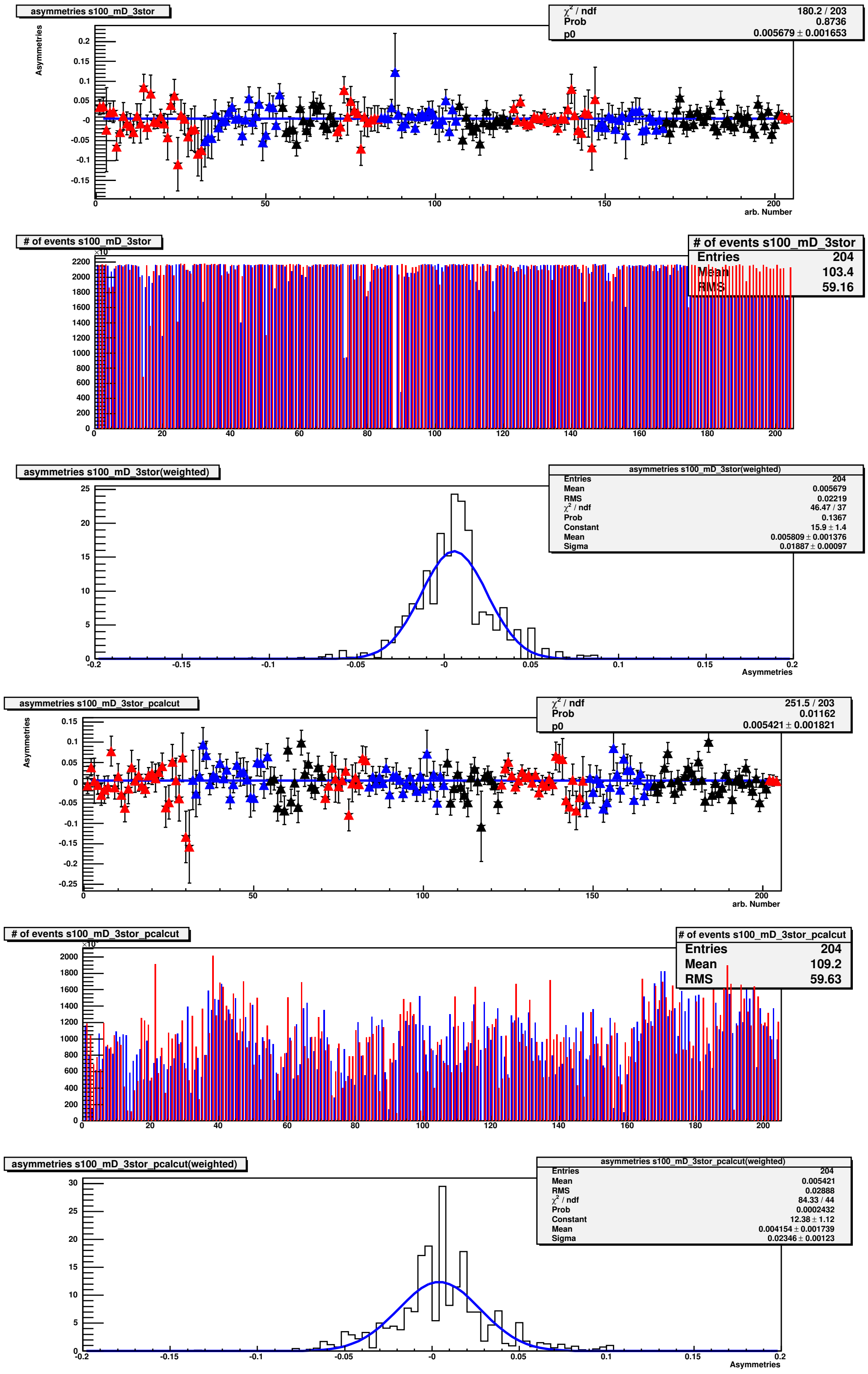

Figure 12: *Same plots as in Figure 10 but using method D for background subtraction. Top before, and bottom after additional application of Cut2.*

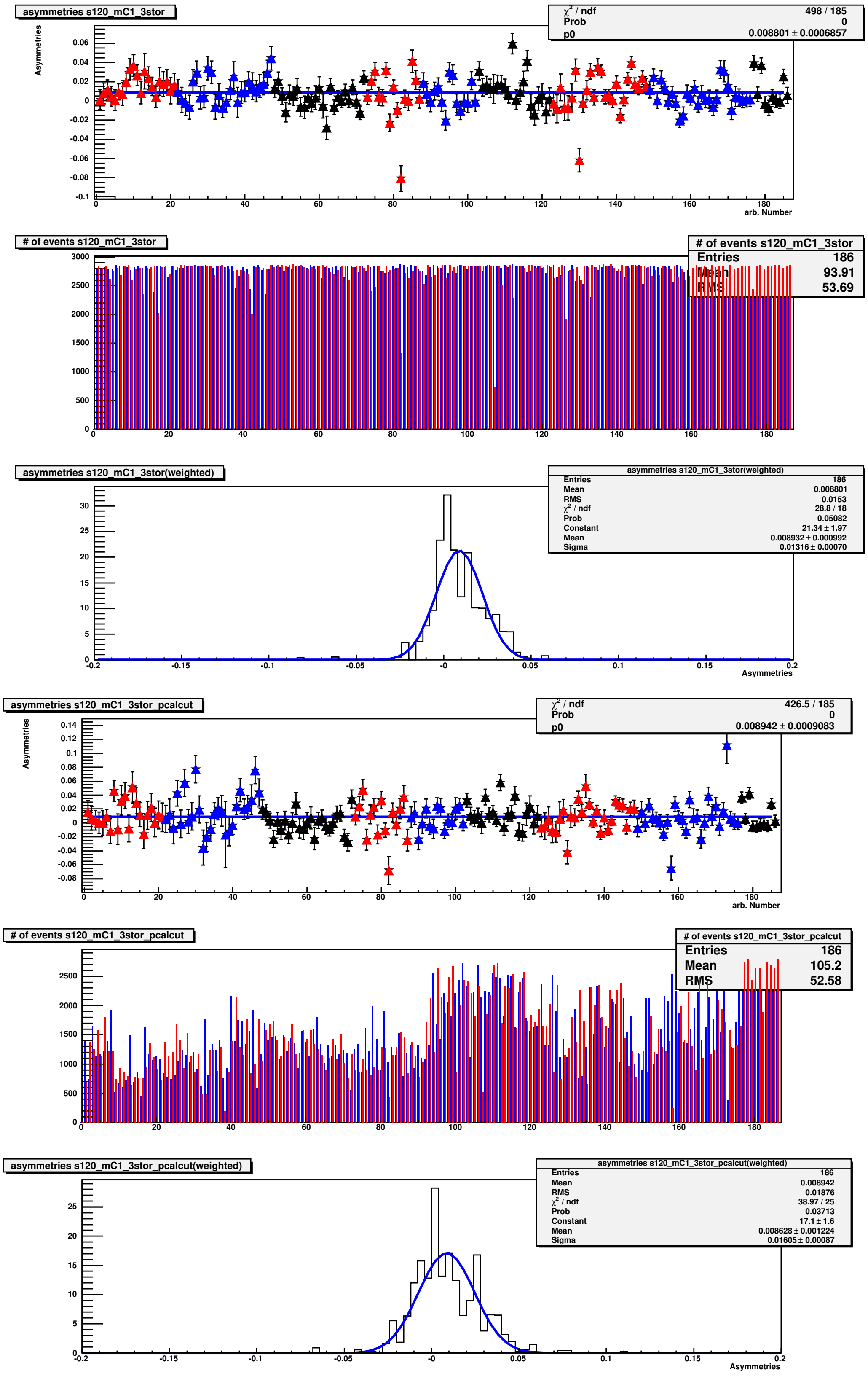

Figure 13: *The asymmetries for the Spec:120, method C1. Top before, and bottom after additional application of Cut2.*

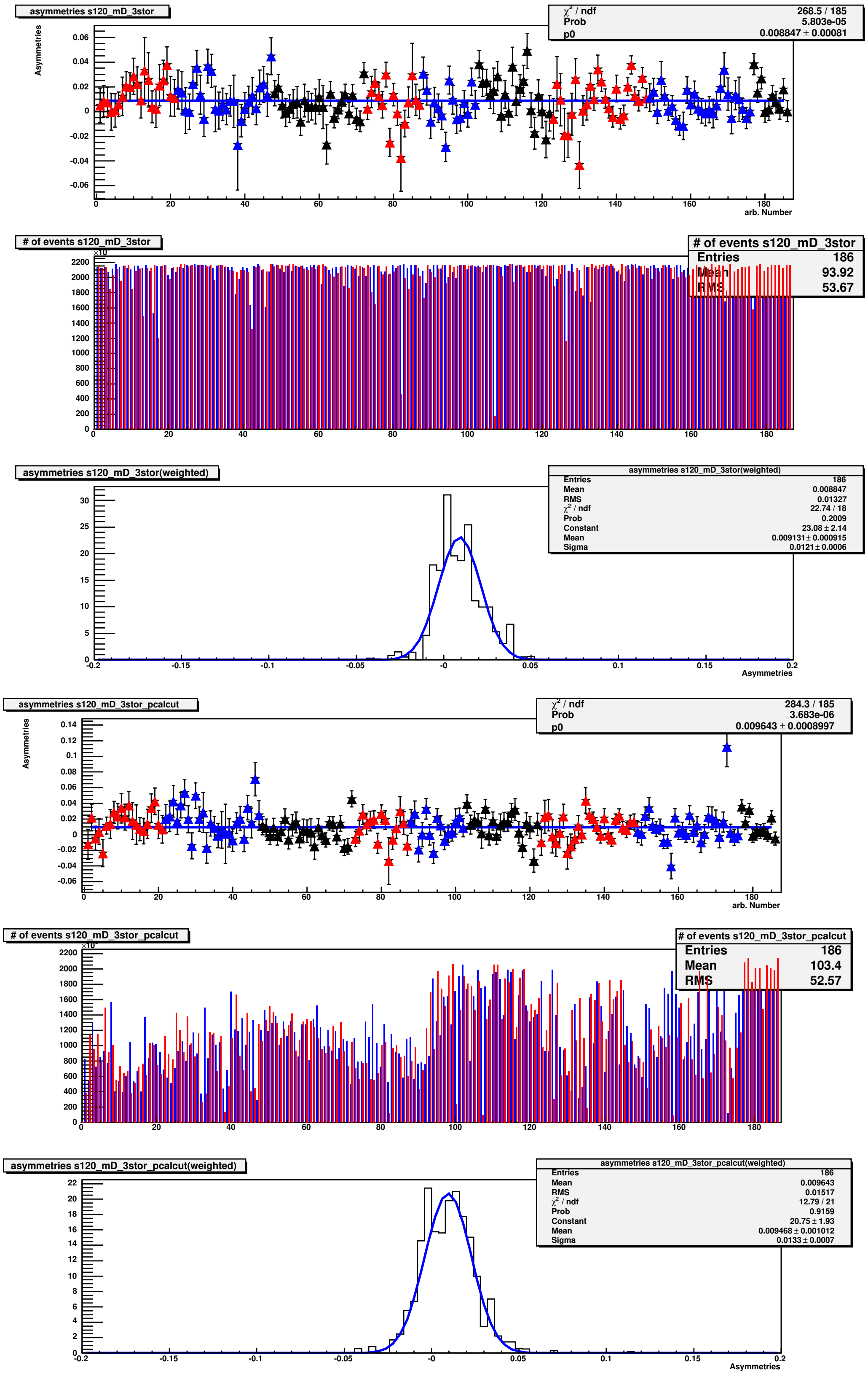

Figure 14: *Same plots as in Figure 13 but using method D for background subtraction. Top before, and bottom after additional application of Cut2.*

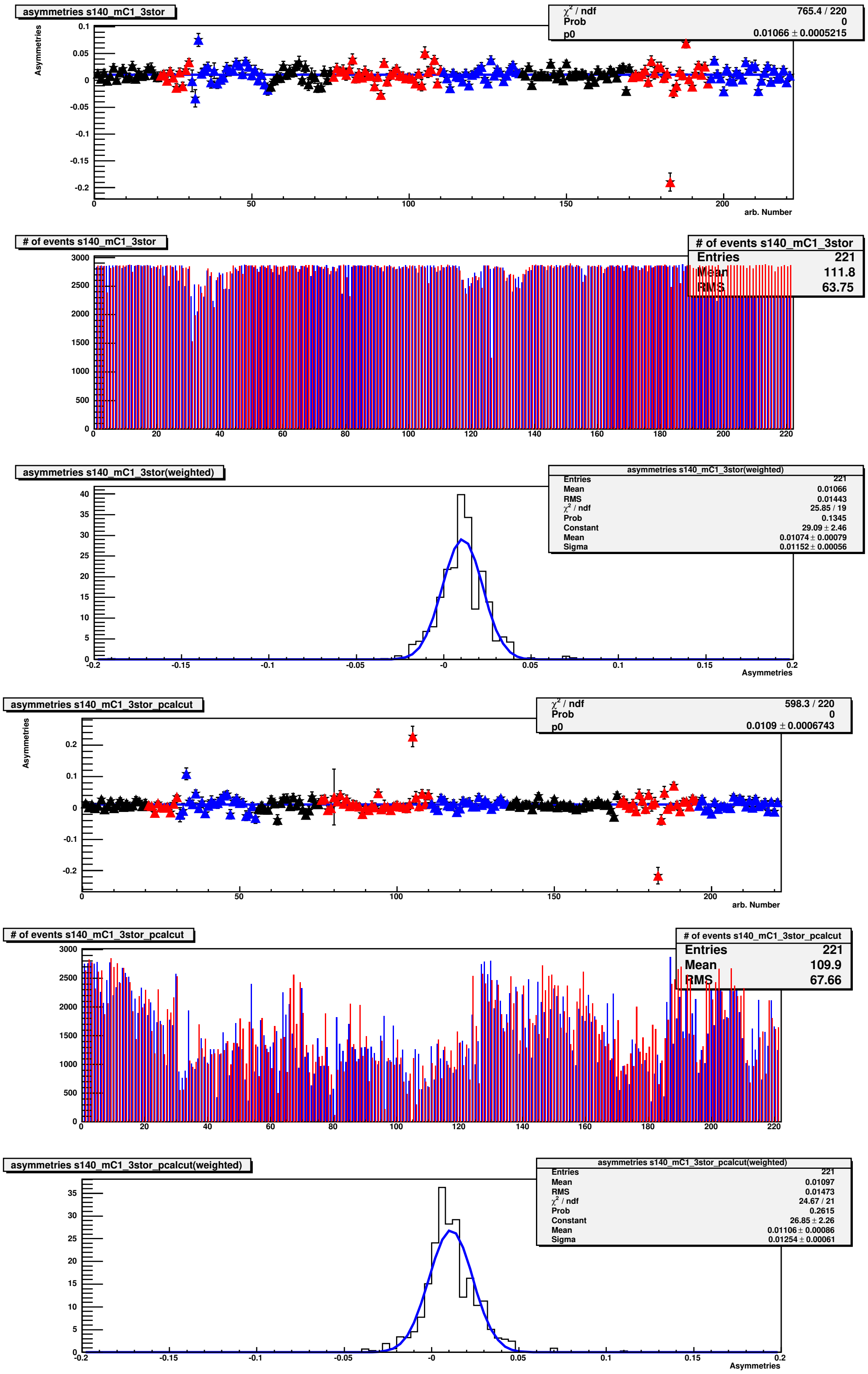

Figure 15: *The asymmetries for the Spec:140, method C1. Top before, and bottom after additional application of Cut2.*

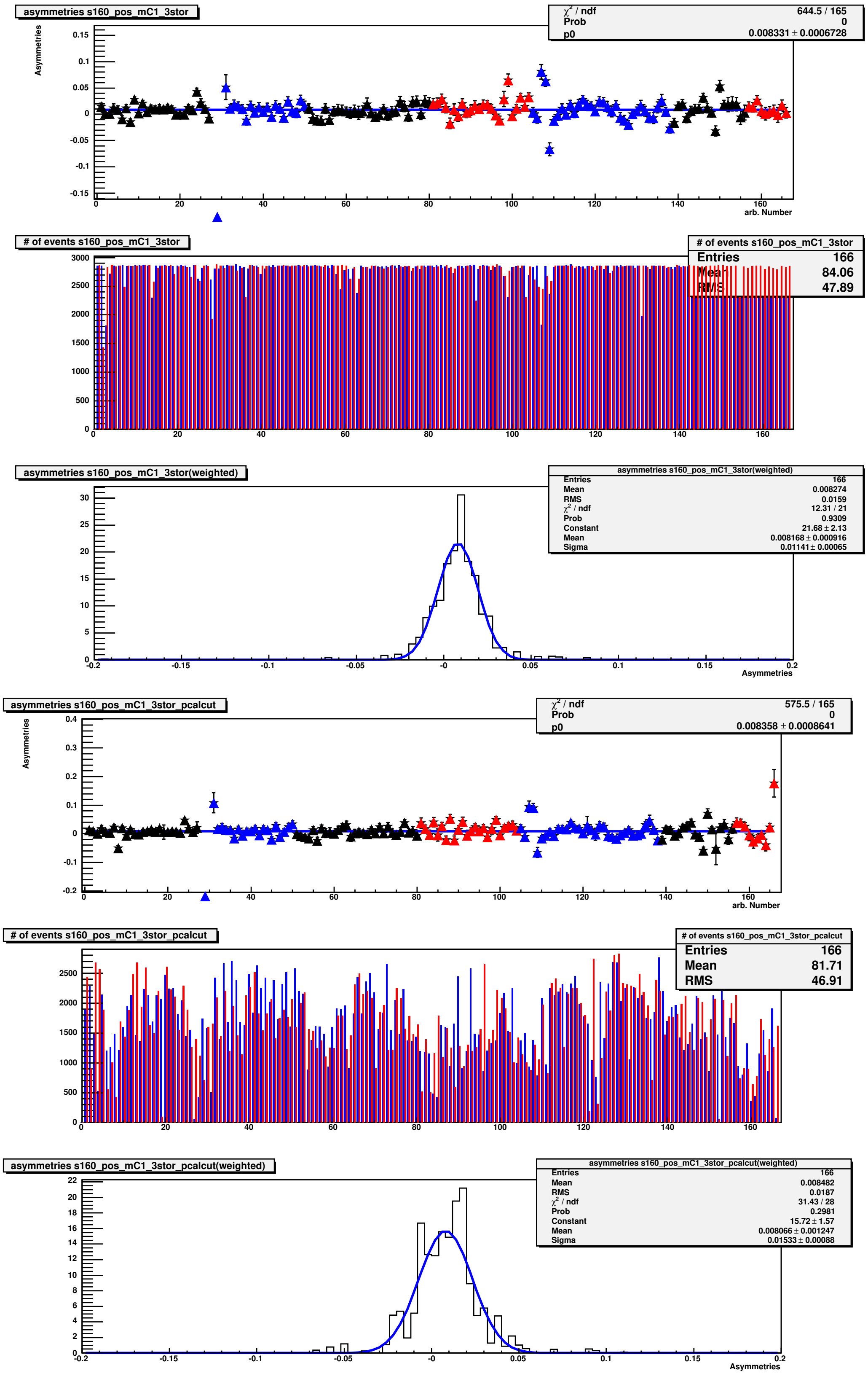

Figure 16: *The asymmetries for the Spec:160pos, method C1. Top before, and bottom after additional application of Cut2.*

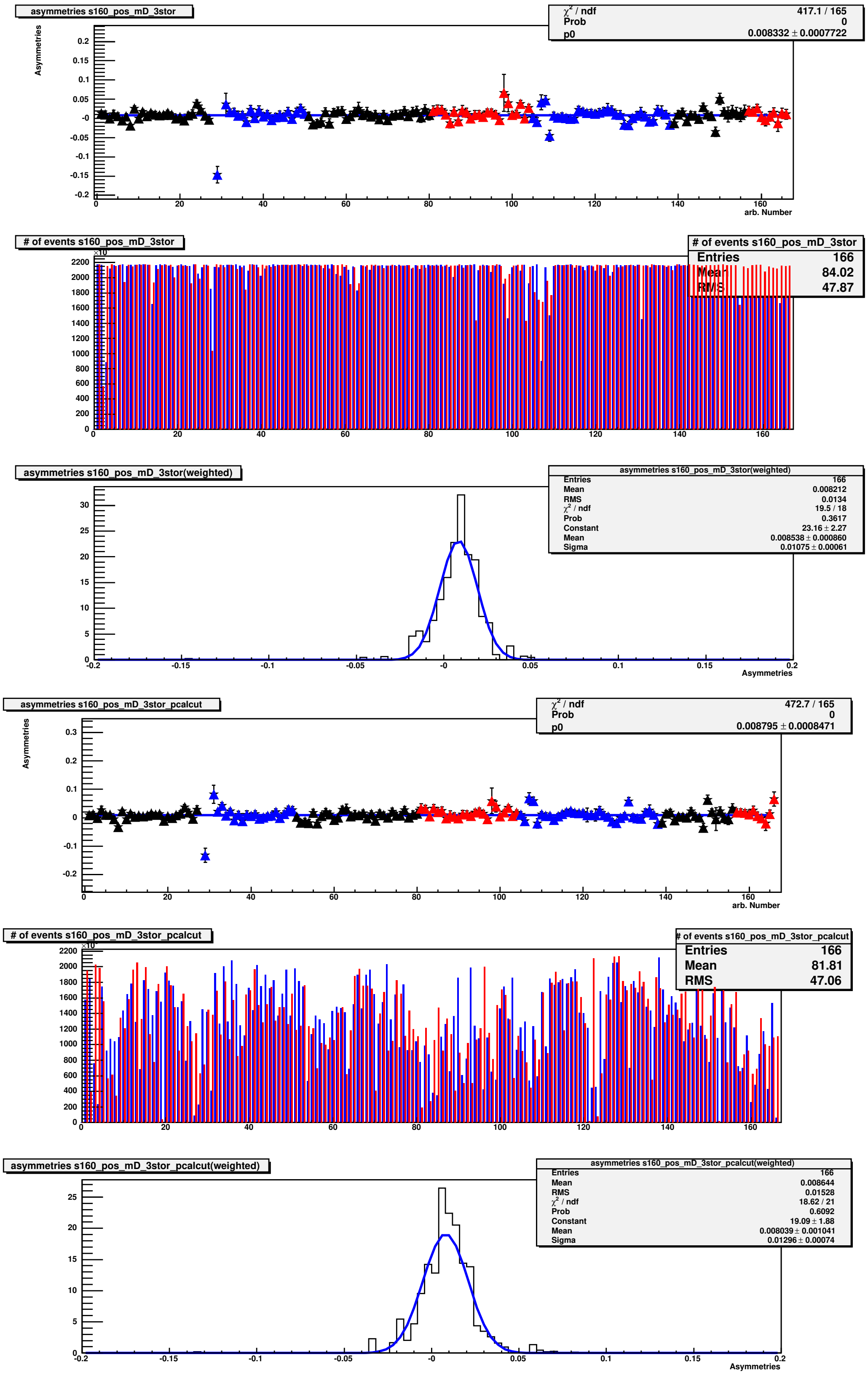

Figure 17: *Same plots as in Figure 16 but using method D for background subtraction. Top before, and bottom after additional application of Cut2.*

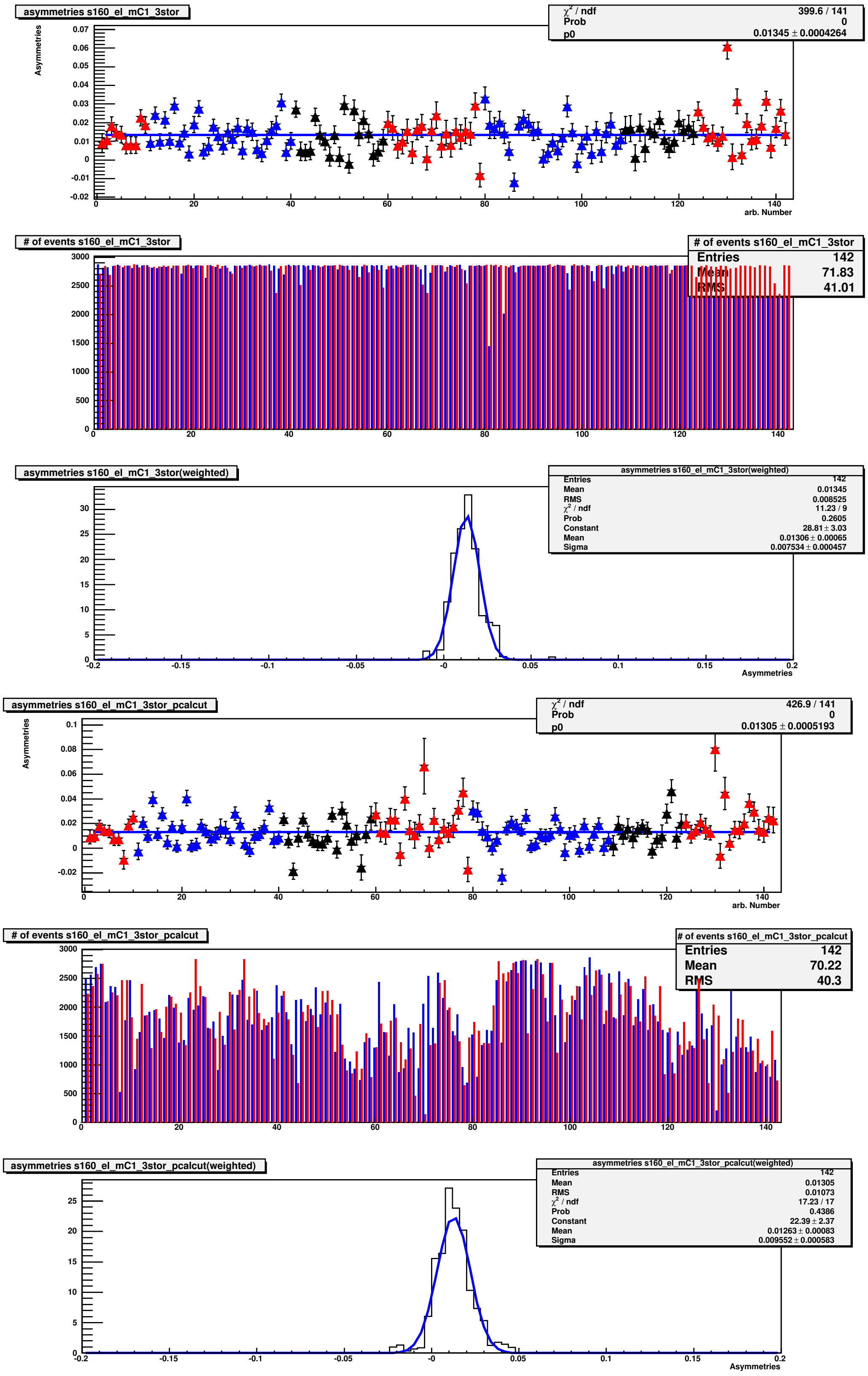

Figure 18: *The asymmetries for the Spec:160el, method C1. Top before, and bottom after additional application of Cut2.*

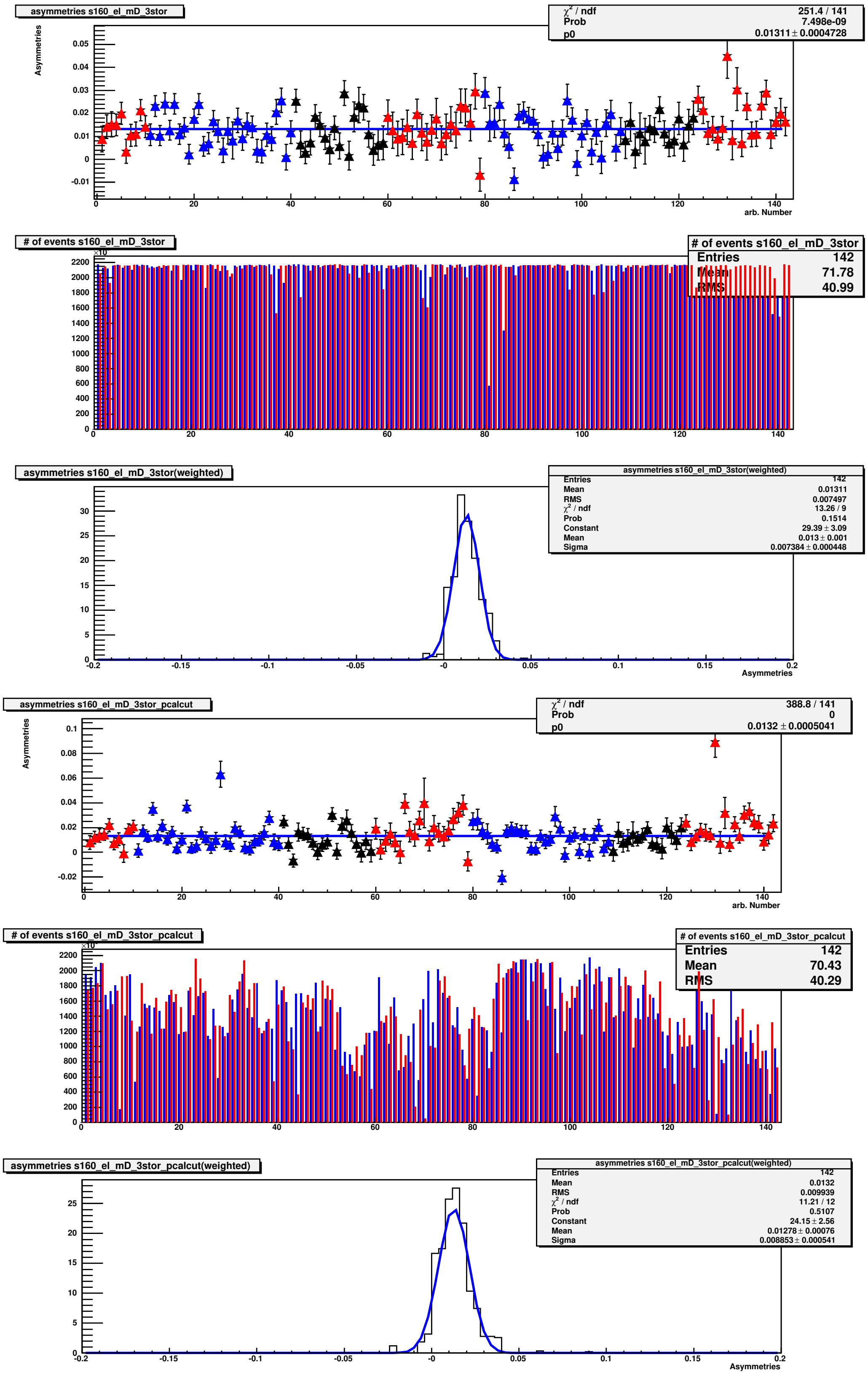

Figure 19: *Same plots as in Figure 18 but using method D for background subtraction. Top before, and bottom after additional application of Cut2.*

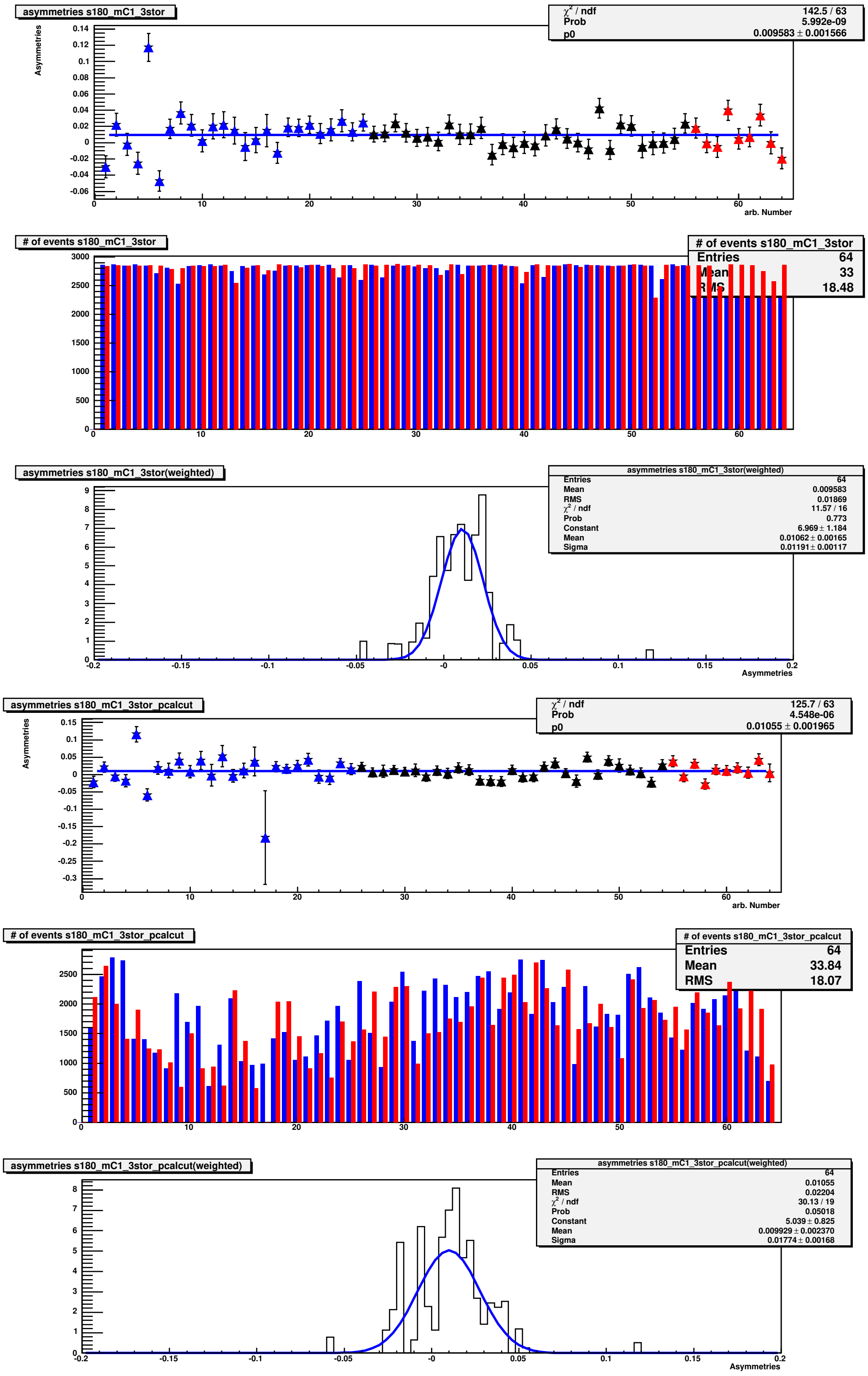

Figure 20: *The asymmetries for the Spec:180, method C1. Top before, and bottom after additional application of Cut2.*

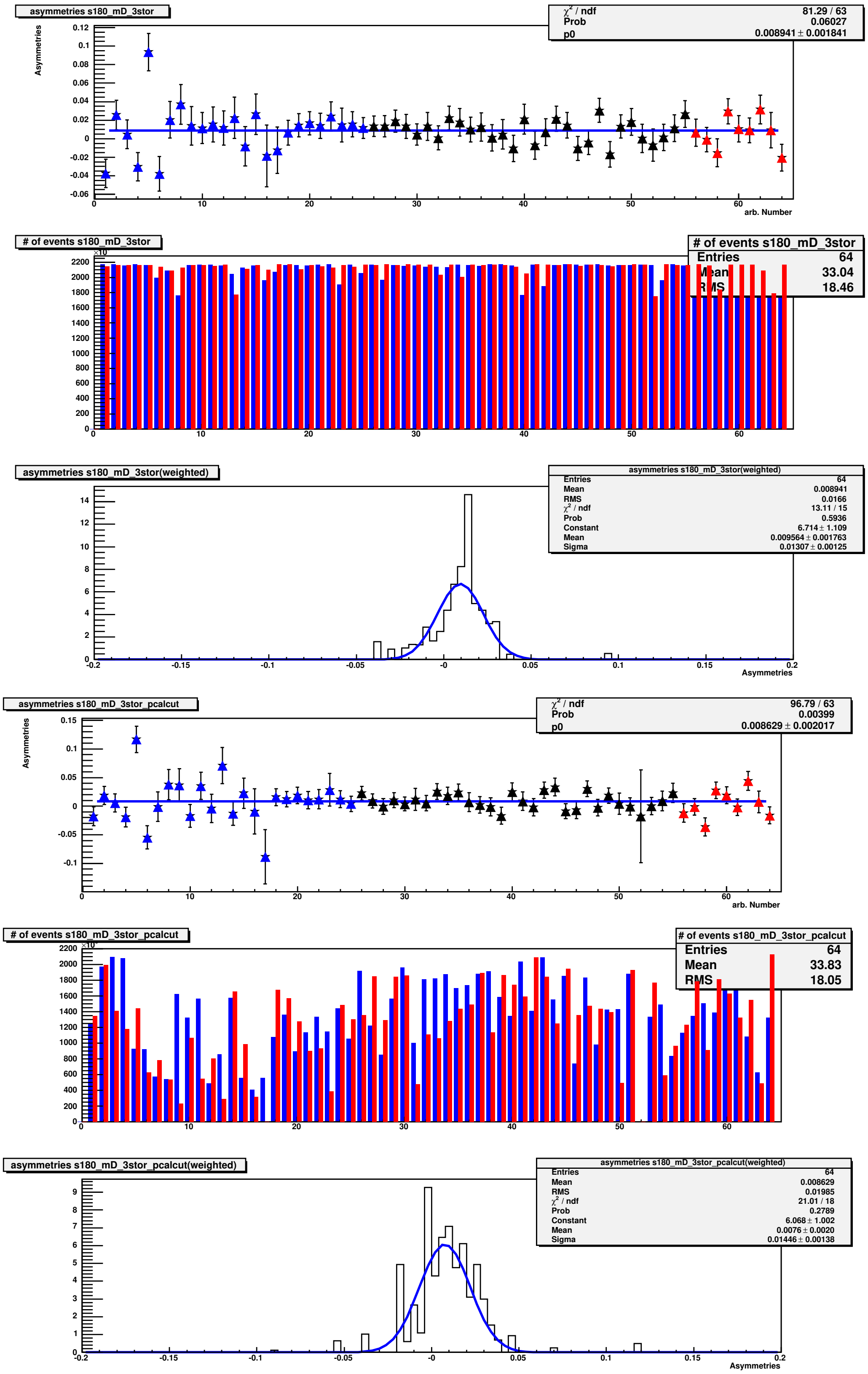

Figure 21: *Same plots as in Figure 20 but using method D for background subtraction. Top before, and bottom after additional application of Cut2.*

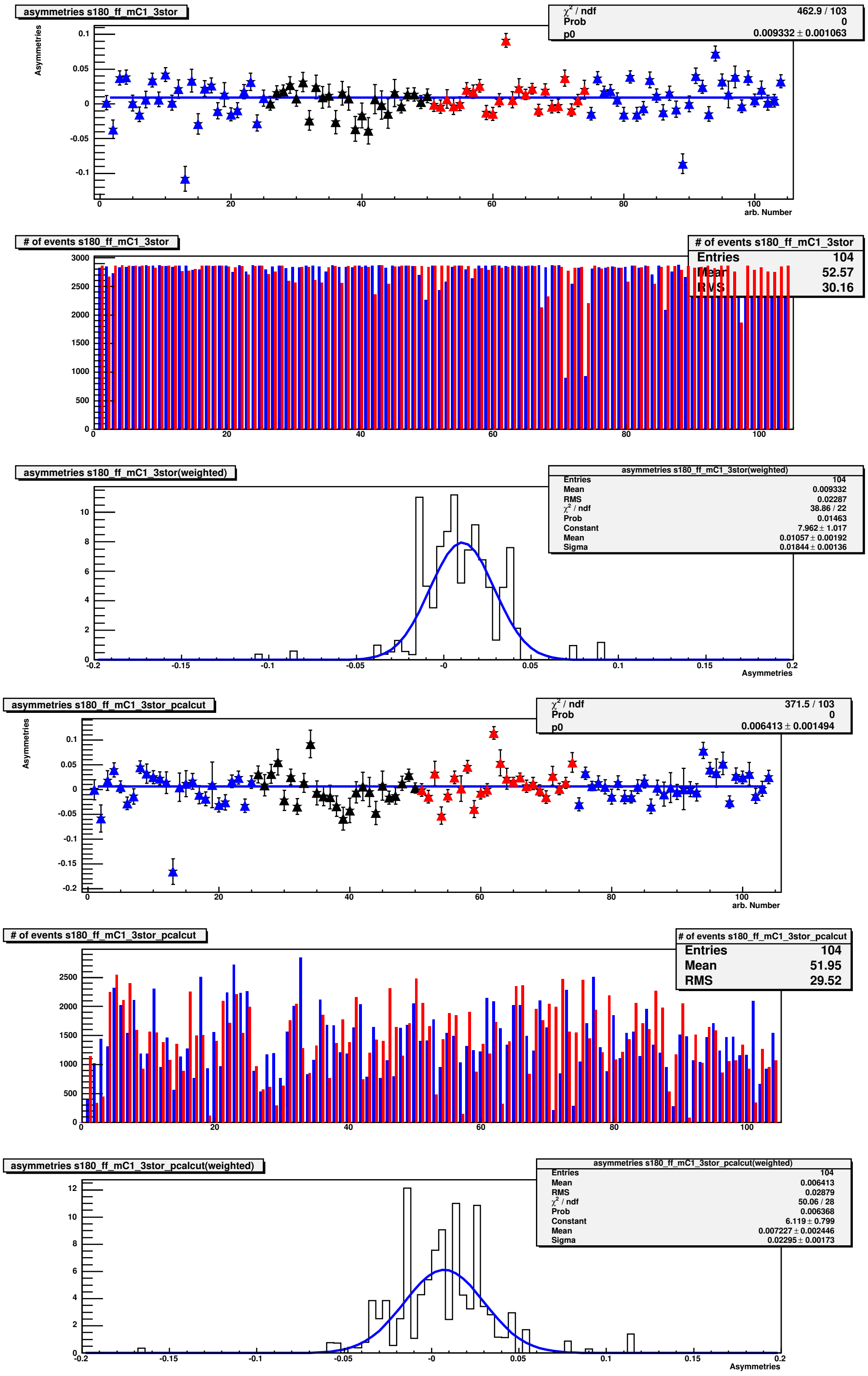

Figure 22: *The asymmetries for the Spec:180-Ferrofluid setting, method C1. Top before, and bottom after additional application of Cut2.*

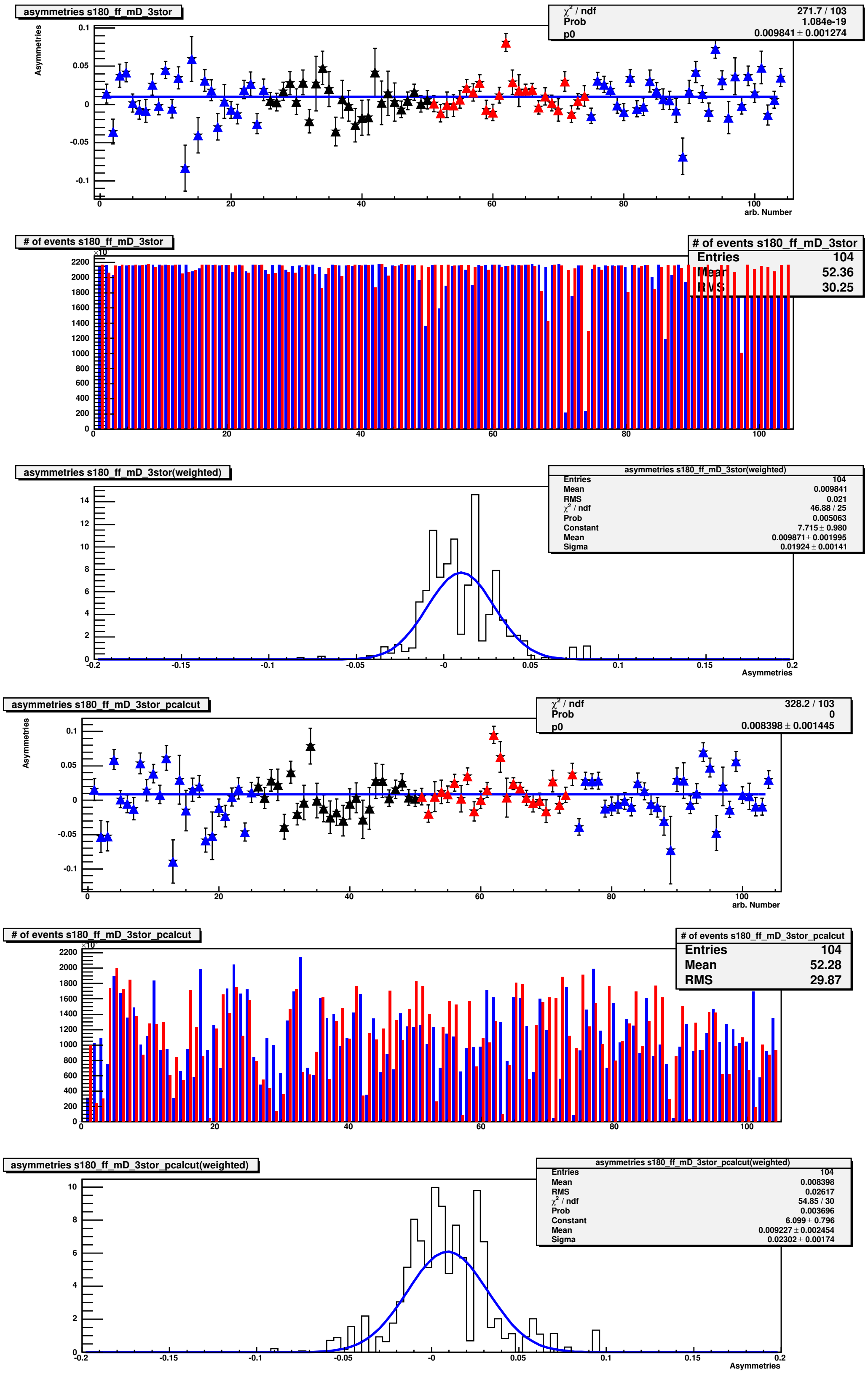

Figure 23: *Same plots as in Figure 22 but using method D for background subtraction. Top before, and bottom after additional application of Cut2.*

B.2 Quality criterion

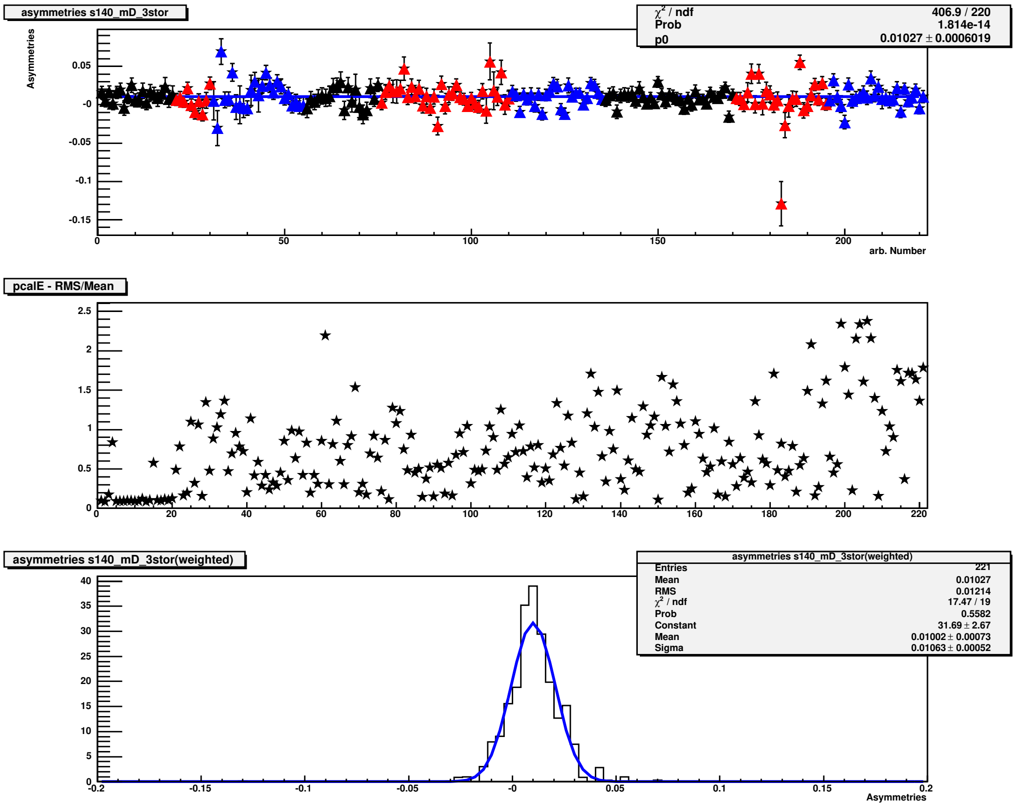

Figure 24: *The single asymmetries for the Spec:140 setting - background subtraction method D + Cut1. There is no selection by the quality criterion, all single asymmetries A_i contribute. Top: The single asymmetries with their errors. Middle: The quality criterion $q = RMS/Mean$ of the distribution in* pcalE. *Bottom: Histogram of the single asymmetries weighted according to Eq.* (11).

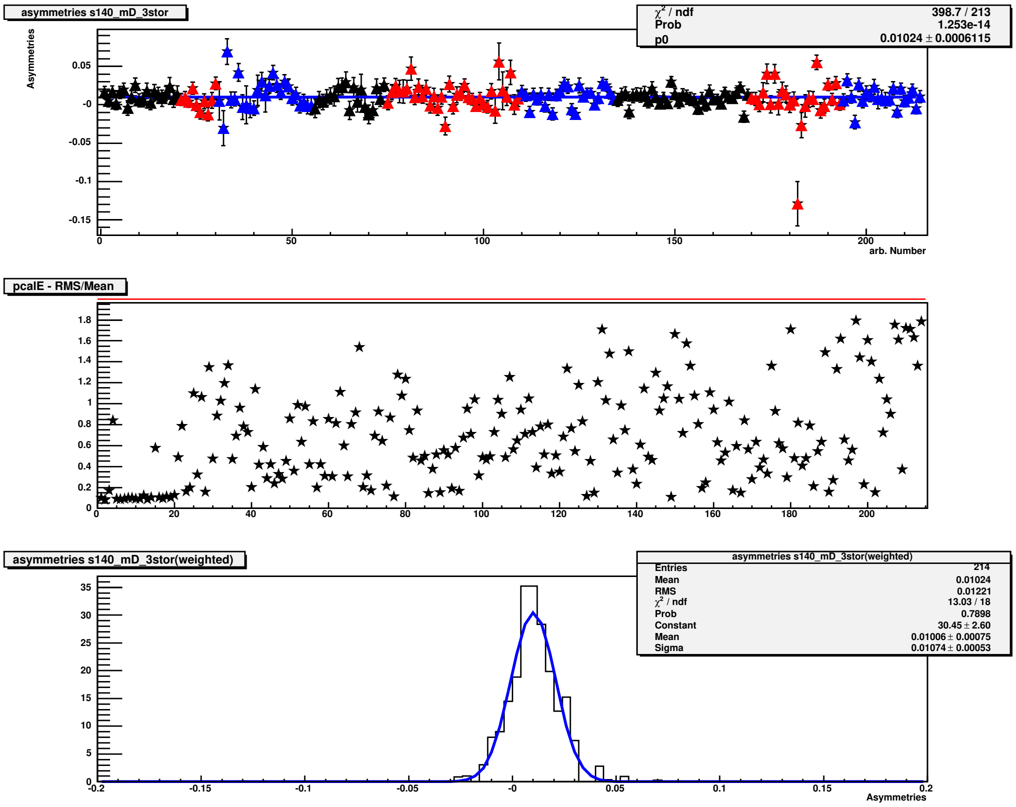

Figure 25: *The single asymmetries for the Spec:140 setting - background subtraction method D + Cut1. The quality criterion is set to 2, asymmetries A_i with the corresponding $q < 2$ contribute. Top: The single asymmetries with their errors. Middle: The quality criterion $q = RMS/Mean$ of the distribution in* pcalE. *Bottom: Histogram of the single asymmetries weighted according to Eq.* (11).

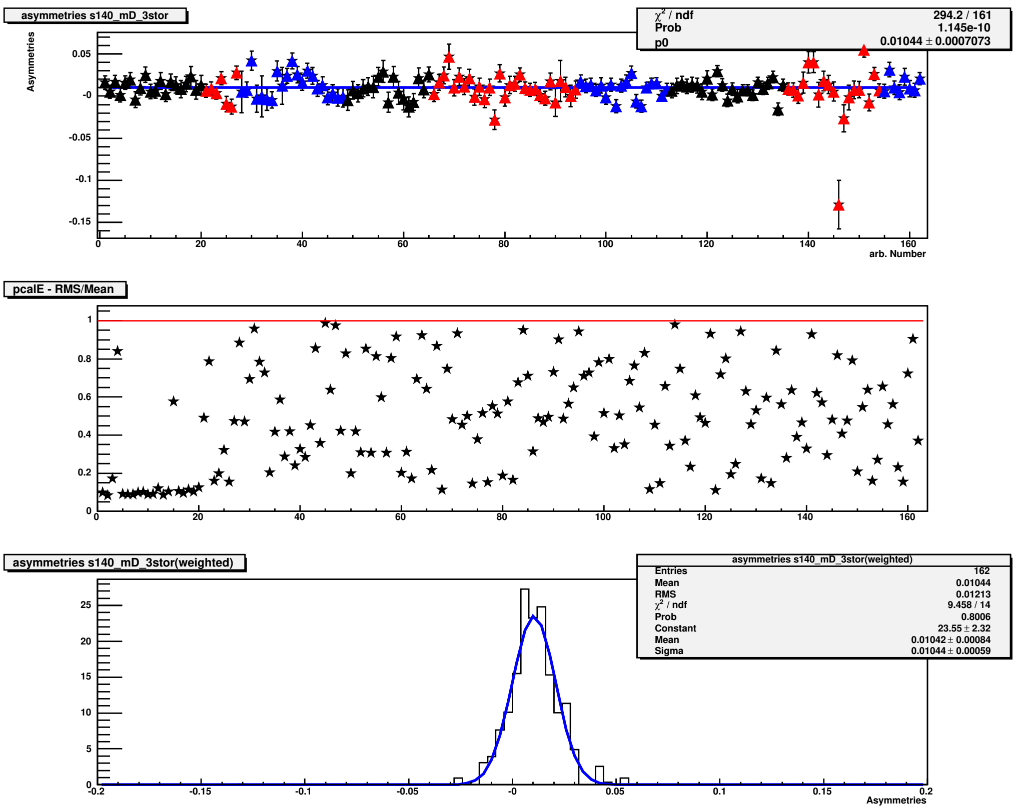

Figure 26: *The single asymmetries for the Spec:140 setting - background subtraction method D + Cut1. The quality criterion is set to 1, asymmetries A_i with the corresponding $q < 1$ contribute. Top: The single asymmetries with their errors. Middle: The quality criterion $q = RMS/Mean$ of the distribution in* pcalE. *Bottom: Histogram of the single asymmetries weighted according to Eq.* (11).

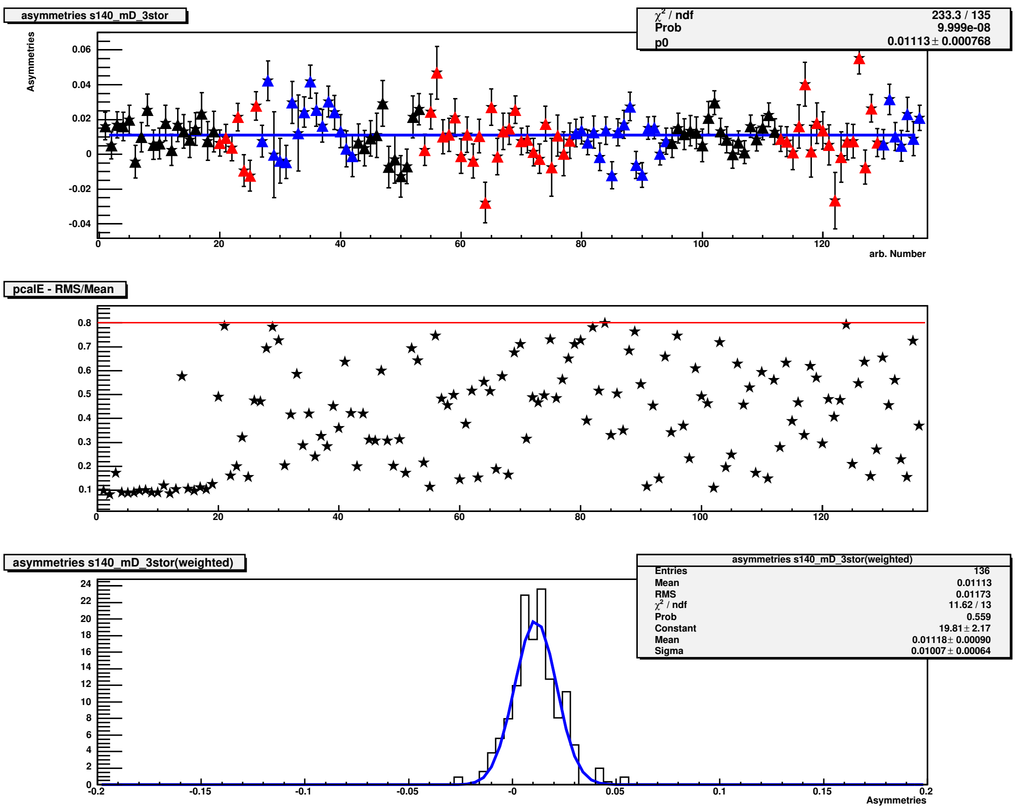

Figure 27: *The single asymmetries for the Spec:140 setting - background subtraction method D + Cut1. The quality criterion is set to 0.8, asymmetries A_i with the corresponding $q < 0.8$ contribute. Top: The single asymmetries with their errors. Middle: The quality criterion $q = RMS/Mean$ of the distribution in* pcalE. *Bottom: Histogram of the single asymmetries weighted according to Eq.* (11).

B.3 Rejection of outliers

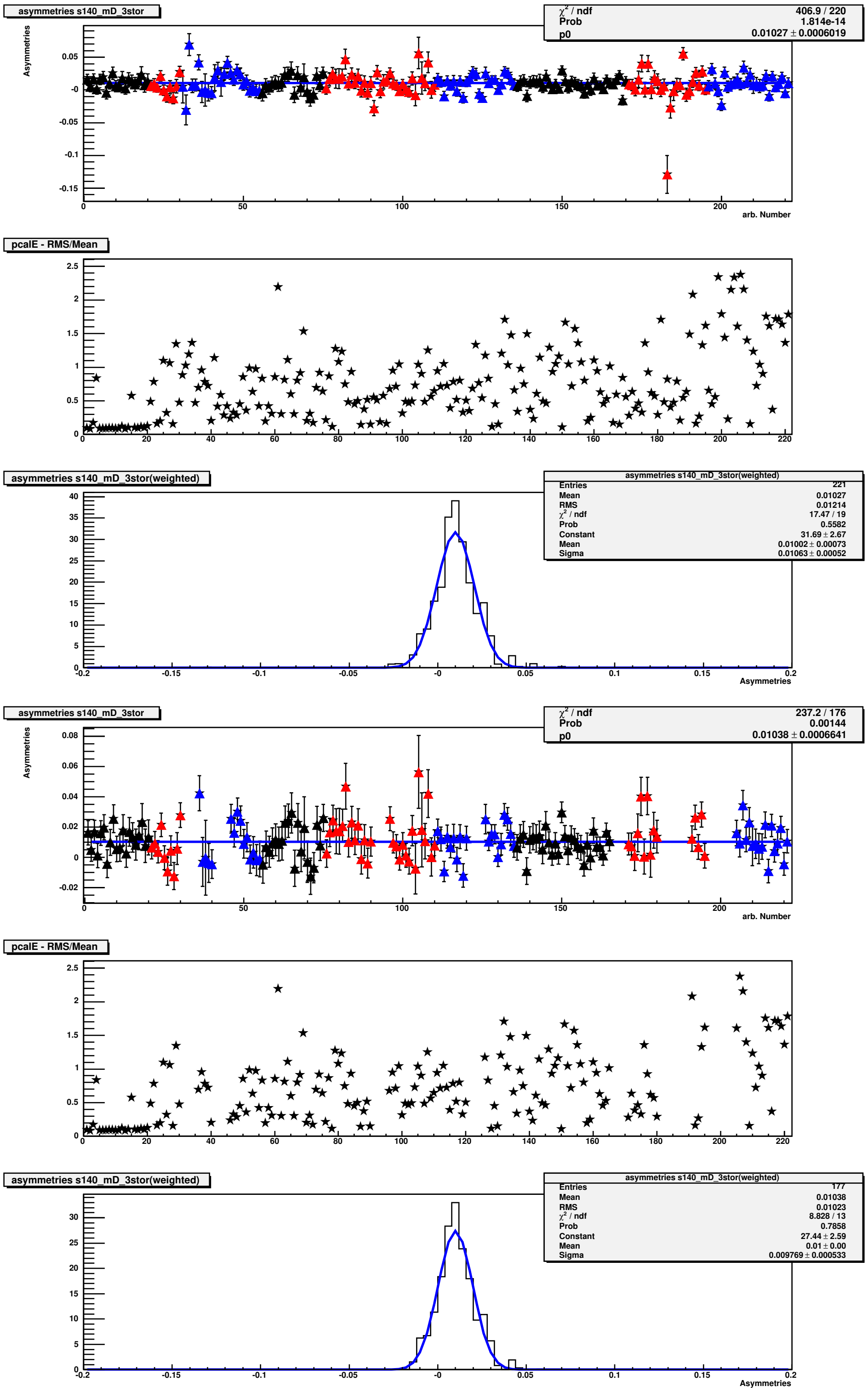

Figure 28: *The asymmetries Spec:140, method D. Top: No run is rejected. Bottom: Runs 2609, 2607, 2625, 2553, 2600, 2558, 2573, 2586 are rejected.*

References

[1] A. Schälicke, H. Kolanoski, S. Riemann, "Analysis of positron asymmetries for June data" E166 Note, September 09, 2005.

[2] R. Pöschel, "Status of the data analysis", talk given at the E166 collaboration meeting in Zeuthen, November 2005.

[3] K. Laihem, "Status of the analysis", talk given at the E166 collaboration meeting in Zeuthen, November 2005.

[4] A. Schälicke, "Robust method for asymmetry analyses", talk given at the E166 collaboration meeting in Zeuthen, November 2005.

[5] E. Reinherz, "Analysis status", talk given at the E166 collaboration meeting in Zeuthen, November 2005.

[6] G. Alexander, E. Reinherz, "Positron asymmetry and polarisation extracted from the E166 September 2005 run" E166 Note, December 19, 2005.

[7] R.J. Barlow, "Statistics: a guide to the use of statistical methods in the physics sciences", John Wiley & Sons Ltd., New York, 1989.